Science of the Total Environment 838 (2022) 156044

Contents lists available at ScienceDirect

Science of the Total Environment

journal homepage: www.elsevier.com/locate/scitotenv

# Combining downscaled-GRACE data with SWAT to improve the estimation of groundwater storage and depletion variations in the Irrigated Indus Basin (IIB)

Arfan Arshad [a,b], Ali Mirchi [a,*], Maryam Samimi [a], Bashir Ahmad [c]

[a] Department of Biosystems and Agricultural Engineering, Oklahoma State University, Stillwater, OK, USA
[b] Department of Irrigation and Drainage, Faculty of Agricultural Engineering and Technology, University of Agriculture Faisalabad, Faisalabad, Pakistan
[c] Climate, Energy and Water Resources Institute (CEWRI) of Pakistan Agricultural Research Council (PARC), Islamabad, Pakistan

## HIGHLIGHTS

- Downscaled-GRACE data improve estimates of groundwater storage (GWS) at fine spatial scales.
- Integrating downscaled-GRACE with results from SWAT helps detect groundwater depletion hotspots.
- GWS changes exhibit significant spatial heterogeneity in the Irrigated Indus Basin.
- Groundwater depletions were higher in the irrigated rice-wheat and cotton-wheat cropping systems.

## GRAPHICAL ABSTRACT

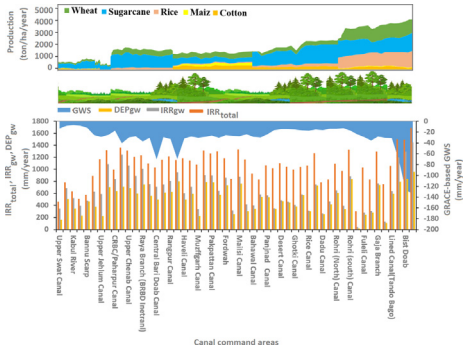


## ARTICLE INFO

Editor: Christian Herrera

*Keywords:*
Soil and water assessment tool (SWAT)
Mixed geographically weighted regression (MGWR)
GRACE
Groundwater depletion
Irrigation
Indus Basin

## ABSTRACT

The growth of agricultural production systems is a major driver of groundwater depletion worldwide. Balancing groundwater supply and food production requires localized understanding of groundwater storage and depletion variations in response to diverse cropping systems and surface water availability for irrigation. While advances through Gravity Recovery and Climate Experiment (GRACE) have facilitated estimating the groundwater storage (GWS) changes in recent years, the coarse resolution of GRACE data hinders the characterization of GWS variation hotspots. Herein, we present a novel spatial water balance approach to improve the distributed estimation of groundwater storage and depletion changes at a spatial scale that can detect the hotspots of GWS variation. We used a mixed geographically weighted regression (MGWR) model to downscale GRACE Level-3 data from coarse resolution (1° × 1°) to fine scale (1 km × 1 km) based on high resolution environmental variables. We then combined the downscaled GRACE-based GWS variations with results from a calibrated Soil and Water Assessment Tool (SWAT) model. We demonstrate an application of the approach in the Irrigated Indus Basin (IIB). Between 2002 and 2019, total loss of groundwater reserves varied in the IIB's 55 canal command areas with the highest loss observed in Dehli Doab by >50 $km^3$ followed by 7.8–49 $km^3$ in the upstream, and 0.77–7.77 $km^3$ in the downstream canal command areas. GWS declined by −325.55 mm/year at Dehli Doab, followed by −186.86 mm/year at BIST Doab, −119.20 mm/year at BARI Doab, and −100.82 mm/year at JECH Doab. The rate of groundwater depletion is increasing in the canal command areas of Delhi Doab and BIST Doab by 0.21–0.35 m/year. Larger groundwater depletion in some canal command areas (e.g., RACHNA, BIST Doab, and Delhi Doab) is associated with the rice-wheat cropping system, low rainfall, and low flows from tributaries.

* Corresponding author.
*E-mail addresses:* aarshad@okstate.edu (A. Arshad), amirchi@okstate.edu (A. Mirchi), msamimi@okstate.edu (M. Samimi).

http://dx.doi.org/10.1016/j.scitotenv.2022.156044
Received 20 February 2022; Received in revised form 21 April 2022; Accepted 14 May 2022
Available online 20 May 2022

## 1. Introduction

Groundwater sustainability has been greatly influenced by massive pumping in the Irrigated Indus Basin (IIB) (Qureshi, 2020) where average groundwater withdrawal consistently exceeds aquifer recharge (Cheema et al., 2014). The contribution of groundwater has reached 40%–60% of the overall irrigation water supply in the recent decades due to the rapid growth of the agricultural sector, population, and industrial demands (Watto and Mugera, 2016; Arshad et al., 2019; Qureshi and Perry, 2021). The surface irrigation system in the IIB delivers a fixed water allocation to each of the 55 canal command areas rather than adjusting the diversion based on the demand. Increasing food and water demand has exacerbated water scarcity, prompting farmers to drill thousands of tube-wells for irrigation (Janjua et al., 2021). Continuous pumping has resulted in a dramatic drop in the water table and groundwater quality (Watto et al., 2021; Qureshi, 2020). The depletion varies depending upon agricultural land uses, cropping systems, rainfall-induced recharge, and diversion of surface water from canals (Scott and Shah, 2004; Arshad et al., 2008; Cheema et al., 2014; Ahmed and Abdelmohsen, 2018). For example, rice-wheat cropping system generally consumes more water than cotton-wheat (Cheema et al., 2014; Arshad et al., 2019). Furthermore, uneven surface water diversion across the canal commands areas plays an important role in groundwater depletion variation (Simons et al., 2020). Accurate, spatially distributed estimates of groundwater depletion and storage variations are essential to analyze the implications of different cropping systems and distribution of surface water supply for groundwater sustainability.

Previous studies have applied a variety of approaches to estimate groundwater depletion (Bierkens and Wada, 2019), including volume-based methods using hydraulic head data (Scanlon et al., 2012; Wang et al., 2020; Ali et al., 2021), groundwater flow modeling (Liu et al., 2020), and remote sensing assisted water balance methods (Rodell et al., 2018; Wang et al., 2020; Mehrnegar et al., 2021; Ali et al., 2021; Ahamed et al., 2022a, 2022b). Volume-based methods, which are generally the most accurate, and groundwater flow modeling have two major limitations for applications in large basins such as the IIB: (1) collecting extensive groundwater monitoring data from observation-wells throughout the basin is costly; and (2) the data are typically unevenly distributed, limiting the ability to capture the spatial variability of groundwater changes across the basin (Ali et al., 2021; Arshad et al., 2020). Alternatively, remote sensing assisted water balance methods compute the groundwater withdrawal rates and compare these with recharge rates obtained from large-scale global hydrological models (e.g., PCR-GLOBWB (Van Beek et al. , 2011), as well as combined remote sensing and watershed hydrology models such as SWAT (Cheema et al., 2014; Liu et al., 2020).

Using SWAT (Soil Water and Assessment Tool) in conjunction with Gravity Recovery and Climate Experiment (GRACE) data allows distributed estimation of groundwater storage and depletion changes at a spatial scale that can detect the hotspots of GWS variation. SWAT is a semi-distributed watershed simulation model (Arnold et al., 1998) that has been widely applied in agricultural regions to simulate the impacts of crops, point source pollution, and irrigation on watershed hydrology (Tan et al., 2020; Samimi et al., 2020). SWAT has been used to investigate the total water storage variability (Hassan and Jin, 2016; Biancamaria et al., 2019; Li et al., 2021) and shallow groundwater storage at basin scale (Awan and Ismaeel, 2014; Dakhlalla et al., 2016; Liu et al., 2020). GRACE is a joint mission of the National Aeronautics and Space Administration (NASA) and the Deutsches Zentrum für Luft und Raumfahrt (DLR). GRACE (April 2002–June 2017) and GRACE-FO (June 2018–present) data facilitate hydrologic assessments by providing total water storage (TWS) data, including soil moisture, groundwater, canopy water, and water from ice and snow with global coverage every 30 days (Rodell et al., 2007; Feng et al., 2013; Castellazzi et al., 2018). GRACE measures the groundwater storage (GWS) variations driven by natural and human influences (Ahmed et al., 2014; Huang et al., 2015; Chen et al., 2019a, 2019b). GRACE data have been used along with land surface models to quantify groundwater changes over the Indus Basin (Iqbal et al., 2016; Tang et al., 2017; Ali et al., 2021) and other watersheds around the globe (Xiang et al., 2016; Felfelani et al., 2017; Yang et al., 2017; Chen et al., 2019a, 2019b; Ahmed et al., 2021; Hu et al., 2022). Xie et al. (2020) integrated GRACE data with SWAT results to improve the representation of groundwater depletion at basin-scale, accounting for anthropogenic impacts. However, the coarse resolution of GRACE data in basin-scale groundwater assessments hinders localized understanding of groundwater storage and depletion variations (e.g., canal command areas in the IIB).

GRACE Level 2 products are available at a spatial resolution of ~3° × 3° which were then processed at gridded level to release Level 3 products represented by three spherical harmonic solutions (with spatial resolution of 1° × 1°) and two mascon solutions (with spatial resolution ranging 0.5°–0.25°) (Watkins et al., 2015; Wiese et al., 2016). We chose to use Spherical Harmonic (SH) from Jet Propulsion Laboratory (JPL) because this product has been shown to have less uncertainty than Mascon products when estimating water storage (Ali et al., 2022), which is why it is widely applied in the Indus Basin (e.g., Iqbal et al., 2016; Tang et al., 2017; Hussain et al., 2020; Ali et al., 2021; Akhtar et al., 2022). Despite spatial improvements in Level 3 products, the resolution of GRACE products remains too coarse for analyzing groundwater changes over smaller agricultural areas (Śliwińska et al., 2021; Ali et al., 2021). Further, Level 3 products with improved resolution contain no more physical information than the native GRACE datasets (Watkins et al., 2015; Gemitzi et al., 2021). Downscaling GRACE-SH data to a fine spatial resolution (~1 km) will make it suitable for small scale applications (e.g., catchments to canal command areas) with improved physical information (Vishwakarma et al., 2021; Ali et al., 2021).

Common downscaling approaches include linear models (e.g., geographically weighted regression (GWR) (Arshad et al., 2021; Wang et al., 2022), partial least squares regression (Vishwakarma et al., 2021)), nonlinear models (e.g., Random Forest model (Ali et al., 2021; Chen et al., 2019)), Artificial Neural Networks (ANN) (Ali et al., 2021)), as well as water balance models (Yin et al., 2018). Among these, the GWR model performs better and uses simplified algorithms for spatial downscaling as compared to other sole regressions (linear, and nonlinear regression models) and machine learning models (ANN and RF) (Zhang et al., 2018; Zhang et al., 2020). However, a common critique of GWR applications is the assumption that the coefficients of variables that predict the dependent variable are always spatially varied, which is not always the case, i.e. the coefficients can be spatially constant for some predictors and varied for others (Gao and Li, 2011; Arshad et al., 2021; Yang et al., 2021). Keeping the coefficients of all predictor variables model spatially varied in the GWR could result in random noise in model prediction (Zeng et al., 2016; Chao et al., 2018; Arshad et al., 2021). To address this limitation, we performed a geographically variability test (GVT) (Arshad et al., 2021) to build a mixed geographically weighted regression (MGWR) model which accounts for mixed interactions, i.e., coefficients can be constant for some predictors and varied for others (Arshad et al., 2021; Yang et al., 2021). The MGWR model handles the spatially varying (local) and constant (fixed terms) coefficients for predictor variables (Arshad et al., 2021). Previous studies have demonstrated that the MGWR model has higher fitting and accuracy than GWR when the regression coefficients of predictor variables are a mix of constant and spatially varying values (Arshad et al., 2021; Yang et al., 2021; Zeng et al., 2016; Chao et al., 2018). Therefore, current study explored the applications of MGWR model to downscale GARCE data from coarse resolution to fine scale (1 km) using high-resolution predictor variables. A set of environmental variables in the IIB were used as predictors (see Section 3.1) based on their regional importance (Ali et a., 2021; Arshad et al., 2020) and effects on water storage variations as documented in previous studies (Chen et al., 2019a, 2019b; Gemitzi et al., 2021; Chen et al., 2021; Ali et al., 2021).

This paper presents a novel remote sensing assisted spatial water balance approach to detect GWS variation hotspots based on improved distributed estimation of groundwater storage and depletion changes. The central hypothesis is that there is great spatial heterogeneity in groundwater

depletion within each of the IIB's 55 canal command areas due to varying levels of anthropogenic activities, irrigation water supply, and types of cropping systems. We quantify high-resolution spatiotemporal groundwater changes (storage and depletion) in the canal command areas by: (a) downscaling GRACE data from coarse resolution (1° × 1°) to fine scale (1 km × 1 km) for distributed quantification of GWS changes over different irrigated plains, and (b) combining the downscaled-GRACE-based GWS data with hydrologic response unit (HRU) results from a calibrated SWAT model to improve groundwater depletion (DEPgw) characterization in different cropping systems and canal command areas. We apply the spatial water balance approach in the IIB to answer the following research questions: (i) how well can we estimate GWS variations over irrigated plains?; (ii) how much groundwater has been depleted in different command areas?; (iii) what causes the decline in GWS and increase in DEPgw?

## 2. Study area

The study area is the IIB, which covers about 490,760 km$^2$ within the Indus Basin (Fig. 1a). The IIB is divided into 8 different irrigated plains (land between two rivers) (Fig. 1b) and 55 canal command areas (Fig. 1c). The basin topography changes from the highest elevation (~8100 m) in the Himalayas to the low-lying areas of Sindh. Surface water in the Indus Basin is provided by the Indus River and its main tributaries (Beas, Ravi, Sutlej, Jhelum, Chenab, and Kabul) which mainly originate from snowmelt and glacial waters at the upstream high-mountain areas of the Himalayas, Karakoram, and Hindu Kush (Immerzeel et al., 2010). The Indus River and its tributaries supply a total of ~175 billion cubic meters (BCM) of surface water annually, of which ~128 BCM is used for surface irrigation; ~12 BCM is lost through system losses and 35 BCM is diverted to the sea (Zuberi, 1997).

The Indus Basin is underlain by a large unconfined aquifer that encompasses about 16 million hectares (ha). Both surface water and groundwater resources contribute to irrigation supply and their contribution varies in each irrigated plain depending on the cropping system, surface water diversion, and groundwater availability. The upper irrigated plains receive a higher percentage of their irrigation from groundwater, whereas the lower plains are more likely to receive water from surface diversions (Fig. 1b&c). The study area covers diverse cropland systems such as rice-wheat, cotton-wheat rotation/orchard, cotton-wheat rotation/sugarcane, rice-fodder, and fodder-wheat (Fig. 1d). The rice-wheat cropping system is more dominant in the south-east regions such as Punjab and Haryana (Gumma et al., 2019). Over the past decades, agricultural intensification has increased crop water use, causing available surface water to fall short of meeting the crop water requirements (Arshad et al., 2019; Qureshi and Perry, 2021).

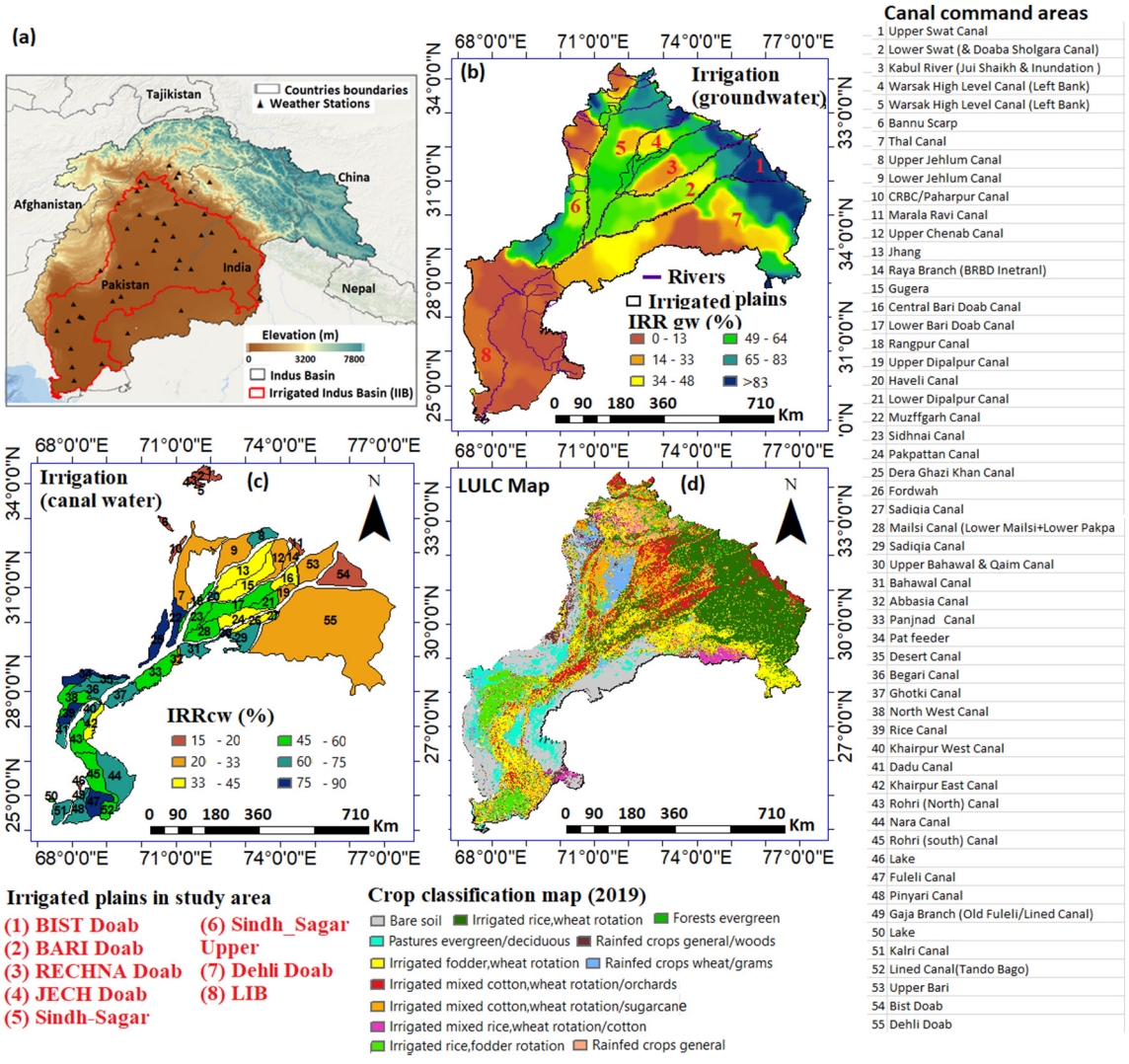


**Fig. 1.** (a) Location of IIB in the Indus basin, (b) percentage distribution of irrigation from groundwater; c) percentage distribution of irrigation from surface water (55's canals), and (d) distribution of cropping systems in the IIB for year 2018–2019.

## 3. Materials and methods

### 3.1. Input data

We used different data streams including satellite observations, reanalysis, model outputs, and ground-based observational data. Details of data used in the current study are provided below and summarized in Table. 1.

#### 3.1.1. GRACE-based TWS

GRACE-based total water storage anomalies (ΔTWS) have been processed by different centers, namely CSR (Center for Space Research), GFZ (German Research Center for Geosciences), and JPL (Jet Propulsion Laboratory) (Landerer and Swenson, 2012). TWS comprises surface and subsurface storage compartments such as surface water, soil moisture, snow, ice, groundwater, and canopy water (Chen et al., 2016). GRCTellus Land RL05 release of GRACE data from these centers are available in two different solutions, spherical harmonic (SH) and mascon. We used monthly GRACE-based TWS of spherical harmonic solution (JPL-SH) available at 1° × 1° resolution from 2002 to 2019 (https://grace.jpl.nasa.gov/data/get-data/monthly-mass-grids-land/). The months for which GRACE observations were missing were filled by linear interpolations and averaging the values of two months before and after the month with missing data as suggested by previous studies (Ali et al., 2021; Long et al., 2015). Scaling factor was applied to restore the original signal in GRACE data that was lost during the pre-processing (Seyoum et al., 2019).

#### 3.1.2. GLDAS data

Monthly data of soil moisture storage (SMS), canopy water storage (CWS), surface runoff (Qs), and snow water equivalent (SWE) were taken from GLDAS (Global Land Data Assimilation System) version CLSMv2.0 with a spatial resolution of $0.25^0 \times 0.25^0$. These variables were further resampled to a finer scale (1 km × 1 km) using the cubic resampling approach in ArcGIS (Chao et al., 2018).

#### 3.1.3. Environmental variables

Environmental variables were used as predictors for downscaling of GRACE data include elevation, soil moisture storage (SMS), canopy water storage (CWS), precipitation (Precip), wind speed, cloud cover, normalized difference vegetation index (NDVI), land surface temperature (LST), and actual evapotranspiration ($ET_a$). The elevation data at spatial resolution of 90 m × 90 m were obtained from SRTM (Shuttle Radar Topography Mission) and upscaled to 1 km × 1 km using cubic interpolation in ArcGIS (Chao et al., 2018). Monthly NDVI data from MODIS onboard Terra sensor (MOD13A3) were obtained at 1 km × 1 km resolution from LPDAS (Land Processes Distributed Active Archive Center). Eight-day daytime and nighttime average LST data from MOD11A2 were retrieved from LPDAC at a spatial resolution of 1 km × 1 km. Monthly mean LST was derived by averaging each 8-day daytime and nighttime LST images. Monthly $ET_a$ from MODIS was obtained from USGS FEWS NET Data Portal which is produced using SSEBop (Operational Simplified Surface Energy Balance) model (Senay et al., 2007). High resolution gridded precipitation data at 1 km × 1 km resolution were retrieved from a previous study which has been validated with ground observations for the Indus Basin (Arshad et al., 2021). Monthly data for cloud cover and wind speed (at 10 m height) of ERA-interim were obtained from European Centre for Medium-Range Weather Forecasts (ECMWF). The native spatial resolution of data is 0.75° × 0.75°, however, ECMWF web applications server (https://apps.ecmwf.int/datasets/data/interim-full-moda/levtype=sfc/) provides user-specified spatial resolutions ranging 3°–0.125° based on bilinear interpolation technique (Liu et al., 2018; Shu et al., 2021). We collected ERA-interim data at 0.125° × 0.125° spatial resolution, and resampled them to 1 km × 1 km resolution using cubic interpolation in ArcGIS (Chao et al., 2018).

#### 3.1.4. Ground-based hydro-meteorological observations

Climate data (including precipitation, temperature, wind speed, and humidity) for 42 weather stations and 3 stream gauging stations were gathered from the Punjab Meteorological Department (PMD) from 1990 to 2019. Depth to groundwater table (DTWT) for 1489 observation wells was obtained from the Punjab Irrigation Department (PID), Lahore, Pakistan. The canal water diversions (surface water supplies) data for each canal command area were collected from various sources including Punjab Irrigation department (PID), and Indus Water Commission (IWC), Lahore, Pakistan, as well as literature (Cheema et al., 2014). The water supply values for each canal were divided by the corresponding total area (A) to obtain surface irrigation supplies ($IRR_{cw}$).

#### 3.1.5. Soil and land use maps

Soil data and land use were used to parameterize the SWAT model. Land-use/land-cover (LULC) map was prepared from normalized difference vegetation index (NDVI) of MODIS (terra and aqua sensors) at a spatial (temporal) resolution of 250 m (8 days). We used a crop phenological approach to classify the study area into 24 distinct classes using unsupervised ISODATA clustering technique (Masud and Bastiaanssen, 2017; Gumma et al., 2019), which were subsequently recoded into 12 main classes based on spectral NDVI profiles (See Fig. S1 in Supplementary Material). Accuracy assessment of land use map was performed by recording data for 172 points from existing maps and Google Earth (Masud and Bastiaanssen, 2017; Gumma et al., 2019; Awan and Ismaeel, 2014) to evaluate the error matrix as described by Cheema and Bastiaanssen (2010) (Table S1 in Supplementary Material). The overall accuracy of the land use map was 82% with average user's and producer's accuracy being 75% and 69%, respectively. The digital soil map for the study area was obtained from the Food Agriculture Organization (FAO), which contains 32 different soil types (See Fig. S1 in Supplementary Material).

**Table 1**
Summary of data used in the study.

| Type | Product | Spatial (temporal) resolution) | Period | Source |
|---|---|---|---|---|
| TWS | GRACE (JPL-SH) | 1° × 1° (monthly) | 2002–2019 | https://grace.jpl.nasa.gov/data/get-data/ |
| SMS, CWS, SWE, Qs | GLDAS | 0.25° × 0.25° (monthly) | 2002–2019 | https://disc.gsfc.nasa.gov/datasets |
| Precipitation | Downscaled TRMM | 1 km × 1 km (monthly) | 2002–2019 | Arshad et al. (2021) |
| ETa | MODIS | 1 km × 1 km (monthly) | 2002–2019 | https://earlywarning.usgs.gov/fews/product/460 |
| NDVI | MOD13A3 | 1 km × 1 km (monthly) | 2002–2019 | https://lpdaac.usgs.gov/dataset_discovery/modis |
| LST | MOD11A2 | 1 km × 1 km (8 days) | 2002–2019 | NASA Land Processes Distributed Active Archive Center |
| Elevation | SRTM | 90 m × 90 m | | http://www2.jpl.nasa.gov/srtm/ |
| Cloud cover | ERA-interim | 0.125° × 0.125° (monthly) | 2002–2019 | http://apps.ecmwf.int/datasets/data/interim-full-moda/ |
| Wind speed | ERA-interim | 0.125° × 0.125° (monthly) | 2002–2019 | http://apps.ecmwf.int/datasets/data/interim-full-moda/ |
| Climate data | Ground-observations | stations (daily) | 1990–2019 | PMD (Pakistan Metrological department) |
| Surface irrigation | Ground-observations | Seasonal | | PID (Punjab Irrigation Department), Indus Water Commission (IWC), and (Cheema et al., 2014) |
| Groundwater level | Ground-observations | Stations (Seasonal) | 2003–2019 | PID (Punjab Irrigation Department) |
| Soil types | FAO | Polygons | | FAO (https://data.apps.fao.org/map/catalog/srv/eng/catalog.search#/metadata/446ed430-8383-11db-b9b2-000d939bc5d8) |

### 3.2. Methods

We applied two independent methodologies (1) spatial downscaling for improving GRACE-based GWS data, and (2) SWAT model and pixel-based water balance approach for groundwater depletion estimates (Fig. 2). Groundwater storage changes (GWS) were estimated from the GRACE data, which were then downscaled to 1 km × 1 km. We combined the downscaled GRACE-based GWS variations with results from a calibrated SWAT model to estimate the groundwater depletion in the IIB's different canal command areas.

#### 3.2.1. Spatial downscaling

The MGWR model was used to downscale GRACE-based TWS changes from 1° × 1° to 1 km × 1 km. The MGWR model is an extension of the GWR which handles spatially varying and fixed (constant) coefficients for the predictor variables in the downscaling framework (Nakaya, 2015; Arshad et al., 2021). Mathematical expression of the MGWR is as follows:

$$Y_i = \sum_{l=1}^{n} \gamma_l Z_{l\,i} + \sum_{K=1}^{P} \beta_k(u_i, v_i)\, x_{ik+\varepsilon\,(u_i,v_i)} \quad (1)$$

where $Y_i$ is the predicted values of dependent variable (TWS in our case); $Z_{l\,i}$ is the $l$th predictor variable with fixed regression coefficient $\gamma_l$ and i = 1, 2, 3, …. , n. $X_{ik}$ represents the kth predictor variable with spatially varying regression coefficient ($\beta_k$) over spatial locations ($u_i$, $v_i$). The error term in the model is represented by $\varepsilon$ ($u_i$, $v_i$).

The model coefficients were estimated using weight matrix by applying the Bi-square kernel function (see equation S1 and S2 in Supplementary Material). The geographical variability test (GVT) was performed to identify the spatially fixed and varying coefficients for the predictor variables in the model (Arshad et al., 2021). In the first step, local regression model (GWR model) was fitted over each prediction location with all variables having spatially varying coefficients. Then, new sets of models were tested by keeping one variable constant (fixed) while the coefficients of other variables were assumed to vary spatially. If the tested models attained better performance than the local GWR model, a model comparison criterion such as AICc (Akaike information criterion) would be smaller and, in turn, DIFF (i.e., Diff of Criterion) would be positive, suggesting that the tested variable has no spatial variability and vice versa (Nakaya, 2015; Zeng et al., 2016; Arshad et al., 2021). Nakaya (2015) showed that if DIFF values are between −2 and 2 the model judgement is weak and higher positive values (>2) suggest that the coefficient of the tested variable should not vary spatially. By contrast, lower negative values of DIFF (< −2) indicate that the coefficient of the predictor variable of interest should vary spatially. This process was repeated for each variable to finally confirm their spatially fixed and varying coefficients to build the MGWR model.

The variable importance (VIMP) test was performed in random forest (RF) model to investigate the settings and importance of different environmental variables in the study region (Ali et al., 2021). VIMP values close to zero show that the variable has less influence while the higher values indicate the greater importance of the variable to explain the variations in water storage.

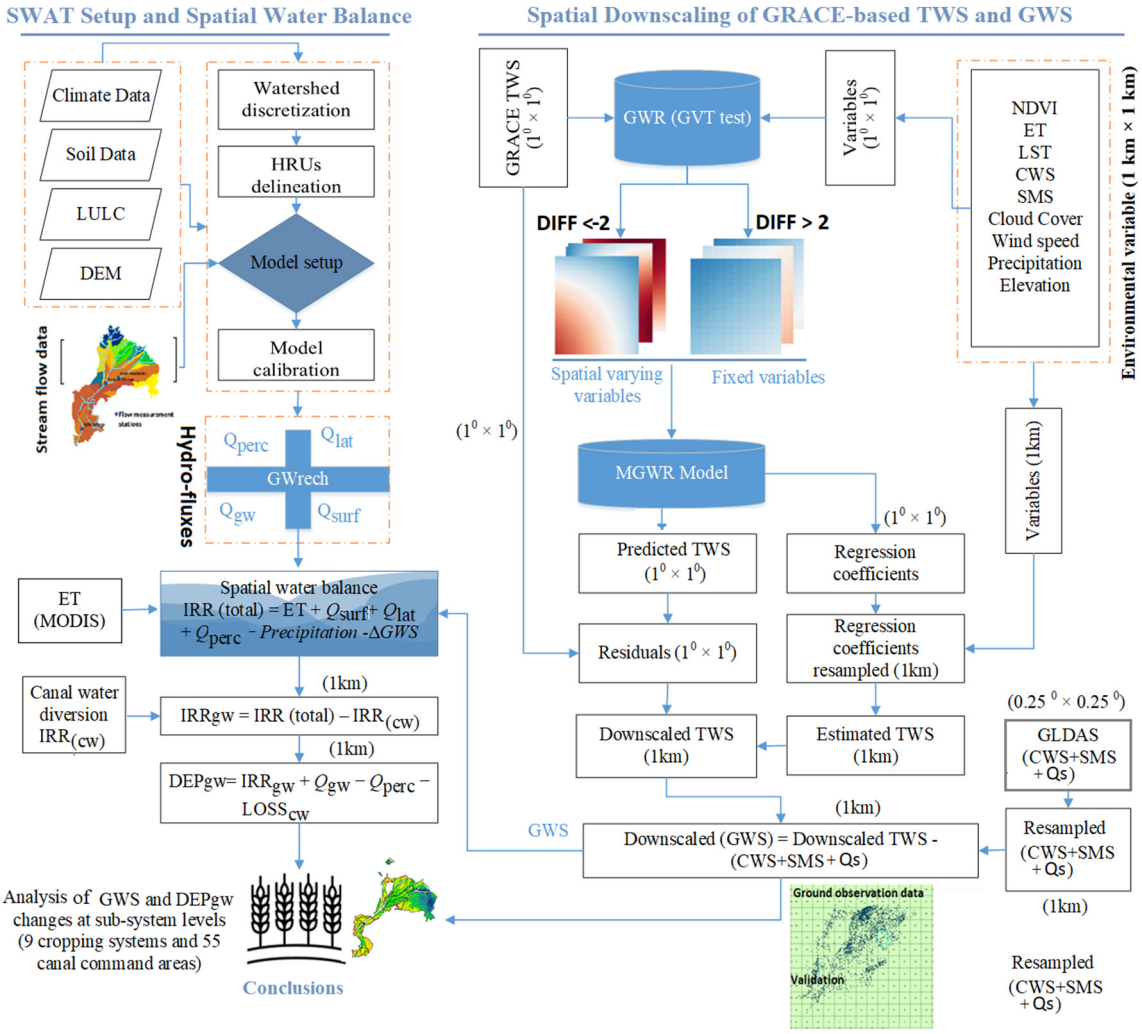


**Fig. 2.** Schematic of the framework, including SWAT model setup, downscaling of GRACE-based GWS, and groundwater depletion estimation in the IIB.

A fundamental premise of the spatial downscaling approach is that spatial relationships established between GRACE-based TWS and environmental variables at a coarse spatial scale can be used to estimate the TWS at finer scale using higher-resolution predictor variables (Jing et al., 2016; Duan and Li, 2016; Arshad et al., 2021). The specific steps of MGWR-based downscaling of GRACE-TWS are summarized in Fig. 2 and explained below.

1. All environmental variables (ET, LST, elevation, NDVI etc.,) at fine resolution (1 km × 1 km) were spatially resampled to coarse resolution (1° × 1°) using cubic interpolation.
2. A MGWR model was built to establish the spatial relationships between GRACE-based TWS (1° × 1°) and environmental variables (1° × 1°) to predict the TWS at 1° × 1° using the following expression:

$$TWS^{1^o}(u_i, v_i) = \sum_{l=1}^{n} \Upsilon_l Z_{l\,i} + \sum_{K=1}^{P} \beta_k{}^{1^o}(u_i, v_i)\, x_{ik}{}^{1^o}(u_i, v_i) + \varepsilon^{1^o}(u_i, v_i) \quad (2)$$

where $TWS^{1o}(u_i, v_i)$ represents the predicted TWS at coarse resolution. The model coefficients (β) for each variable were estimated using weight matrix with Bi-square kernel function. Model coefficients were spatially interpolated from 1° to 1 km resolution using ordinary kriging approach (Duan and Li, 2016).

3. The predicted $TWS^{1o}(u_i, v_i)$ was subtracted from GRACE-based TWS (1° × 1°) to obtain the model residuals (ε) . These residuals were subsequently interpolated to 1 km × 1 km resolution using ordinary kriging approach (Duan and Li, 2016).
4. Downscaled TWS (1 km × 1 km) were obtained using high-resolution environmental variables (1 km × 1 km) in conjunction with model coefficients (1 km × 1 km) and residuals (1 km × 1 km) using following expression.

$$TWS_{downscaled}{}^{1^{km}}(u_i, v_i) = \sum_{l=1}^{n} \Upsilon_l Z_{l\,i} + \sum_{K=1}^{P} \beta_k{}^{1^{km}}(u_i, v_i) x_{ik}{}^{1^{km}}(u_i, v_i) + \varepsilon^{1^{km}}(u_i, v_i) \quad (3)$$

### 3.2.2. High-resolution groundwater storage estimates

Terrestrial water storage comprises of combined contributions from the surface water storage (SWS), groundwater storage (GWS), soil moisture storage (SMS), snow and glacier. Based on the assumption that snow and glacier contribution in the IIB are negligible, GWS is estimated by substrcting the surface runoff ($Q_S$), soil moisture storage (SMS), and canopy water storage (CWS) from the TWS (Ali et al., 2021; Ali et al., 2022; Iqbal et al., 2016; Tang et al., 2017). The following equation was used to derive the groundwater storage variations in the study area.

$$\Delta GWS_{downscaled} = \Delta TWS_{downscaled} \Delta TWS - (\Delta SMS + \Delta CWS + \Delta Qs)_{GLDAS} \quad (4)$$

The contributions of Qs, SMS and CWS were subtracted from the GRACE-based downscaled TWS to obtain the high-resolution GWS estimates. Downscaled GWS was validated with observational data. The data from observation wells are available in the form of depth to water table (DTWT) which is converted into groundwater storage variations by applying the approach suggested by Iqbal et al. (2016) as follows:

1. GTWT is converted into groundwater level (GWL) by subtracting it from depth to bedrock (DTB) [DTB = Depth to bedrock (Average DTB for study area = 400 m)]
2. GWL is converted to anomalies (GWLA) by subtracting the long-term mean (i.e., 2004–2009) similarly to the GRACE anomaly.
3. Finally, groundwater storage anomalies (GWSA) were calculated by multiplying GWLA with specific yield (Sy) [Average Sy for the study area is 0.12 (Iqbal et al., 2016; Bennett, 1967)]

### 3.2.3. SWAT model and pixel-based groundwater depletion

*3.2.3.1. SWAT-model setup.* The IIB was divided into 50 sub-basins, which were further divided into 3032 HRUs (hydrological response units) based on unique combinations of slope, 12 land-use types, and 23 soil types. The water balance equation in the SWAT model simulates spatial variability of surface runoff ($Q_{surf}$), lateral flow ($Q_{lat}$), baseflow entering the main channel ($Q_{gw}$), evapotranspiration (ET), water storage (S), recharge ($GW_{rech}$) to shallow and deep aquifers, and percolation ($Q_{perc}$) (Neitsch et al., 2011; Cheema et al., 2014). Climate data from 42 weather stations were used to parameterize the model from 1991 to 2019. The first three years (1991–1993) were used as a warm-up period to initialize the model parameters. Information about agricultural practices such as sowing, harvesting, and irrigation depths were obtained from Pakistan Agricultural Research Council (PARC, 1982), Cheema, et al., (2014), and Ahmad (2009). The SWAT calibration and uncertainty procedures (SWAT-CUP) was used to calibrate (1994–2002) and validate (2002–2019) the model with streamflow data from Islam, Panjnad, and Kottri gauging stations, and potential ET data. The NSE (Nash-Sutcliffe efficiency coefficient) and $R^2$ (coefficient of determination) were used to evaluate the model's performance (Moriasi et al., 2007).

*3.2.3.2. Pixel-based groundwater depletion.* We applied a pixel-based groundwater depletion technique for the IIB proposed by Cheema et al. (2014) to reflect the changes in groundwater abstraction/depletion. The pixel information on $ET_a$ (from MODIS), precipitation (from downscaled-TRMM), groundwater storage changes (GRACE-based downscaled data) when integrated with HRU-scale fluxes obtained from the calibrated SWAT model facilitates quantifying total irrigation water supply ($IRR_{total}$).

$$IRR_{total} = ET_a + Q_{surf} + Q_{lat} + Q_{perc} - \text{Precipitation} - \Delta GWS_{downscaled} \quad (5)$$

It is assumed that the decline in groundwater storage is driven by an increase in irrigation supply. The surface irrigation ($IRR_{cw}$) obtained for different canal command areas (Fig. S2) was subtracted from the $IRR_{total}$ to estimate the amount of groundwater applied to irrigate ($IRR_{gw}$) crops in the study area.

$$IRR_{gw} = IRR_{total} - IRR_{cw} \quad (6)$$

Net groundwater depletion (DEPgw) was estimated for each pixel using pixel information on $IRR_{gw}$, canal water losses (LOSScw), peculation ($Q_{perc}$), and baseflow entering the main channel ($Q_{gw}$) using following expression:

$$DEP_{gw} = IRR_{gw} - LOSScw - Q_{perc} + Q_{gw} \quad (7)$$

### 3.3. Uncertainty analysis

Uncertainty in downscaled TWS is associated with the model's input variables (NDVI, LST, ET, elevation etc.). The uncertainty associated with each input variable was quantified by multiplying their coefficient value (β) by sample standard error obtained from standard deviation (σ) (Duan and Li, 2016). The total uncertainty in MGWR-based downscaled TWS ($\sigma_{TWS}$) was estimated by combining uncertainties associated with each model input parameter using propagation of errors by linearization (Faber, 2002; Duan and Li, 2016; Seyoum et al., 2019) as follows:

$$\sigma_{TWS} = \sqrt{\begin{array}{l}(\beta_1 * \sigma_{NDVI})^2 + (\beta_2 * \sigma_{LST})^2 + (\beta_3 * \sigma_{ET})^2 + (\beta_4 * \sigma_{Elevation})^2 + (\beta_5 * \sigma_{CWS})^2 \\ +(\beta_6 * \sigma_{SMS})^2 + (\beta_7 * \sigma_{Cloud\ cover})^2 + (\beta_8 * \sigma_{Wind\ speed})^2 + (\beta_9 * \sigma_{Precip})^2\end{array}} \quad (8)$$

The coefficient value (β) was computed using the MGWR model (Eq. (3)).

Uncertainties in downscaled GWS (i.e.,$\sigma_{GWS}$) are associated with downscaled GRACE-based TWS data and GLDAS variables (CWS, Qs, SMS). Therefore, uncertainties associated with each variable were estimated by standard deviation (σ) of the values, and subsequently combined by adding

individual uncertainties of TWS, CWS, SMS and Qs in the first-order error propagation (Seyoum et al., 2019; Ahmed, 2020):

$$\sigma_{GWS} = \sqrt{\sigma_{TWS}^2 + \sigma_{CWS}^2 + \sigma_{SMS}^2 + \sigma_{Qs}^2} \quad (9)$$

## 4. Results and discussion

### 4.1. Hydrological fluxes from SWAT

Fig. 3a shows the comparison between simulated and measured stream flows for calibration (1994–2002) and validation (2002–2019) for two gauging stations; one located in the upstream of the study area and another one near the basin outlet. A good agreement is observed based on streamflow upstream of the Islam Headwork station yielding NSE ($R^2$) of 0.69 (0.68) and 0.81(0.83) during the calibration and validation periods, respectively. The statistics are relatively lower near the basin outlet at Kotri with NSE ($R^2$) of 0.61 (0.62) for the calibration period and 0.65 (0.69) during validation because flow is highly regulated by human activities in the downstream regions (Immerzeel and Droogers, 2008). However, model calibration and validation based on streamflow is satisfactory given the values of NSE and $R^2$ within and near the acceptable limits ($R^2$ = 0.60 and NSE = 0.50) as recommended by Santhi et al. (2001) and Moriasi et al. (2007). Further, SWAT-simulated ET values agreed well ($R^2$ = 0.84 and NSE = 0.86) with MODIS-ET from 2003 to 2019. Previous research has established

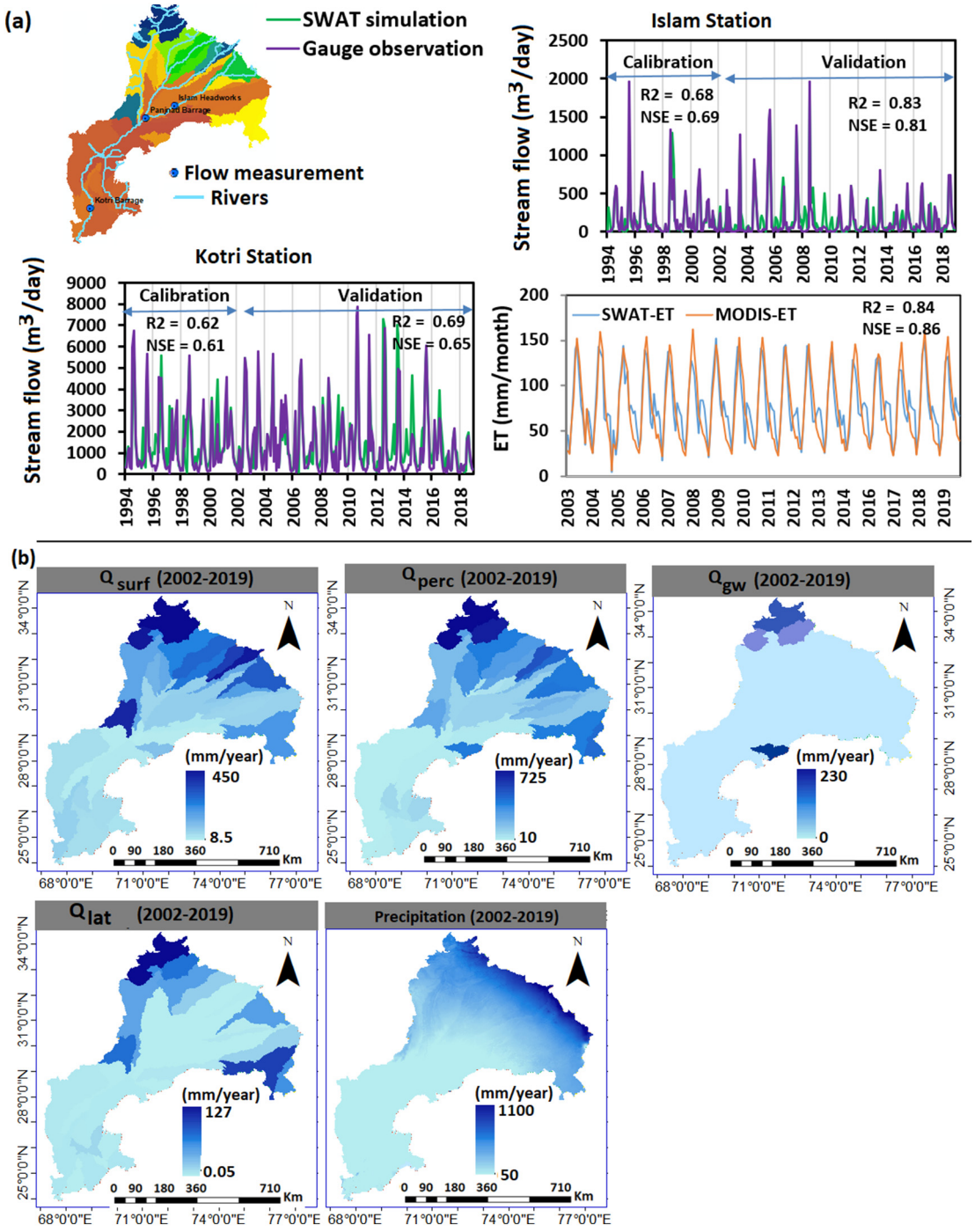


**Fig. 3.** a) SWAT model validation using streamflow data and potential ET; b) average spatial distribution of SWAT hydrological fluxes in the IIB from 2002 to 2019.

acceptable SWAT model performance in various regions of the IIB, with $R^2$ (NSE) ranging from 0.60–0.81 (0.77–0.83) when comparing SWAT-simulated ET with SEBAL-based ET (Cheema et al., 2014; Awan and Ismaeel, 2014; Awan et al., 2016; Becker et al., 2019; Umar et al., 2022). The calibrated SWAT model was used to compute the monthly hydrological fluxes such as surface runoff ($Q_{surf}$), percolation (Qperc), lateral flow (Qlat), and baseflow (Qgw) (See Fig. S3 in Supplementary Material). Fig. 3b represents the spatial distribution of SWAT-simulated hydrological fluxes averaged from 2002 to 2019 in different sub-basins in the IIB. $Q_{surf}$, $Q_{perc}$, and $Q_{lat}$ ranged 8.5–450 mm/year, 10–725 mm/year and 0.05–127 mm/year, respectively, with relatively higher values in the upper sub-basins corresponding to higher amounts of annual precipitation (between 400 and 1100 mm/year). The spatial heterogeneity of $Q_{gw}$ was found to be negligible in the study area. Our findings are consistent with a previous study by Cheema et al. (2014).

### 4.2. Settings of environmental variables and spatial downscaling

The model's ability to estimate high-resolution TWS and GWS variations highly depends on the environmental variables that contribute to changing trends in water storage variations (Ali et al., 2021). As indicated by the VIMP test, the importance of environmental variables varies spatially based on the complex hydroclimatic and topographical features of the study region (Fig. S4). For instance, elevation changes in the lower IIB are more important compared to upstream regions while an opposite trend is observed in the case of CWS, which was found to be more important in model prediction with a VIMP value of 80% followed by Precip (55%), Cloud cover (48%), and NDVI (35%). Table 2 summarizes the results of the GVT test, which included estimates of coefficients and DIFF of Criterion values characterizing the spatially varying and fixed coefficients of the environmental variables in the MGWR model. The coefficients for cloud cover and SMS were introduced as fixed terms into the MGWR model based on their higher positive DIFF values (i.e., 9.29 and 4.90), while other coefficients were input as spatially varying terms.

All the spatially fixed and varying coefficients for the variables at coarse resolution (1° × 1°) were introduced in MGWR to predict the TWS and results were compared with the original GRACE-based TWS from 2002 to 2019. Based on the statistical evaluation of MGWR-based predicted TWS and GRACE-based TWS from 2002 to 2019 (Fig. 5S), the modeling approach under- and over-estimated the TWS with the bias of −2.81% and 9%, respectively, while $R^2$ ranged between 0.77 and 0.89. Pixel wise evaluation indicated that the spatial pattern of TWS predicted by the model closely matches the original GRACE-based TWS with slight under/over estimations in some locations (Fig. S6a and b). The performance of the MGWR model was satisfactory on most grid cells, with $R^2$ values ranging from 0.75 to 0.95 (Fig. S6c). Fig. S6d shows the residual maps which are noise in terms of under- and over- estimation in model prediction and depict the amount of TWS not explained by the model. The maximum under- and over-estimation reported in the model-based TWS compared to the GRACE-based TWS were − 30 mm/year and 30 mm/year, respectively. Further, the model coefficients (1° × 1°) obtained from the MGWR model were interpolated to 1 km × 1 km using the ordinary kriging method (OK) and re-introduced into the MGWR model along with 1 km × 1 km environmental variables to obtain the high-resolution GRACE-based TWS estimates (Fig. S6e). Residual corrections reduce the bias in downscaling results, i.e., over/under-estimation. Residuals correction is performed by combining model residuals with estimated TWS to obtain the downscaled GRACE-based TWS at fine resolution (Fig. S6f). The MGWR produced satisfactory results with high values of $R^2$ and small residuals, denoting that it can be applied to predict high-resolution TWS in the study region with the current setting of environmental variables. The spatial pattern of downscaled TWS closely resembles that of the GRACE-based TWS, indicating that the downscaling technique enhances the spatial information in GRACE data while preserving the spatial pattern of TWS.

Uncertainties in the MGWR-based downscaled TWS result from different error sources (e.g., input variables). Fig. S7 represents the individual uncertainty of each input variable. The total uncertainty in the downscaled TWS was 28.35 mm and associated individual uncertainties were 14.70 mm (LST), 13.54 mm (ET), 12.75 mm (CWS), 11.57 mm (NDVI), 7.55 mm (SMS), 5.85 mm (cloud cover), 2.87 (wind sped), 2.83 mm (Precip), and 0.91 mm (elevation).

Fig. 4 illustrates the spatial changes in TWS (Fig. 4a) and the comparison between monthly GRACE-based and downscaled TWS changes over the IIB (Fig. 4b). The TWS is decreasing from 2002 to 2019, however, the trend is more dominant in South-East regions (Haryana and Punjab (India)) which is associated with high pumping of the aquifer for human consumption and irrigation water supply where GWS is the main component of the TWS. The spatial heterogeneity in TWS variation is also associated with substantial human footprints in the already vulnerable regions as well as dryland characteristics of the study region (An et al., 2021; Zhu et al., 2021). Time series of the coarse GRACE-based data and downscaled results shows a similar variation amplitude and values of TWS are consistent before and after downscaling, indicating that the downscaling approach is suitable to predict TWS changes with current data streams and results (Fig. 4b). It is observed that regional TWS in the IIB declined by −30.45 mm/year (from 2002 to 2009) and −104.78 mm/year (from 2009 to 2019).

Furthermore, subtracting the contribution of surface water storage compartments (SMS, CWS, Qs, and SWE) from TWS is essential to estimate the GWS. The spatial-temporal quantification of GLDAS-based SMS, CWS, Qs, and SWE in the study region indicated that SMS had the highest annual average contribution, ranging between 0 and 300 mm/year, followed by Qs (0–40 mm/year) and CWS (0–0.9 mm/year), while SWE is negligible in the study region. Therefore, GWS estimates were obtained by removing the contributions of SMS, Qs and CWS from the TWS (See Fig. S8 in Supplementary Material).

### 4.3. How well can we estimate GWS variations over irrigated plains?

Fig. 5 contrasts GRACE-based GWS variations with downscaled GWS variations for different irrigated plains in the Indus basin for the year 2019. The 2° (~222 km) P1-P2 transect demonstrates how downscaling improved the estimation of GWS variations within each irrigated plain. The high-resolution GWS data along the transect capture the spatial variation of GWS, which appears as uniform in the coarse resolution GRACE data. For example, downscaled data reflect a strong spatial heterogeneity in the GWS variations (−100 mm to −3000 mm/year) in Dehli Doab with a higher decline observed in upstream regions with predominantly high-density rice-wheat cropping system and greater population growth necessitating large amounts of groundwater withdrawal (Roy et al., 2020). The decline of GWS in Dehli Doab is lower in downstream regions with barren land and low agro-urban activities (Samie et al., 2020) where aquifer salinity levels (total dissolved solids (TDS) range: 3000 to 10,000 mg/L) make groundwater unsuitable for irrigation (Swarzenski, 1968; Khan and Khan, 2020). The high-resolution GWS data are particularly useful for small, irrigated plains. For example, GRACE data provide GWS over BIST Doab and JECH Doab canal command areas in homogenized pixels while the

**Table 2**
Results of geographical variability test (GVT) for environmental variables based on DIFF of Criterion.

| Variables | Estimate | Min | Max | DIFF of criterion |
|---|---|---|---|---|
| Intercept | −2529.63 | −40,857.20 | 11,322.52 | −28.12 |
| Could cover | 3077.82 | −9039.29 | 31,162.19 | 9.29 |
| Elevation | 0.34 | −3.28 | 5.82 | −2.45 |
| Precip | −0.54 | −6.79 | 4.96 | −31.74 |
| LST | 23.06 | −149.47 | 321.28 | −20.44 |
| NDVI | 316.11 | −4156.63 | 13,270.65 | −10.12 |
| CWS | −5579.54 | −57,009.90 | 22,734.51 | −46.69 |
| SMS | 1.84 | −9.25 | 22.05 | 4.90 |
| Wind speed | 47.98 | −2832.10 | 4078.09 | −3.15 |
| $ET_a$ | 0.44 | −5.21 | 20.30 | −79.42 |

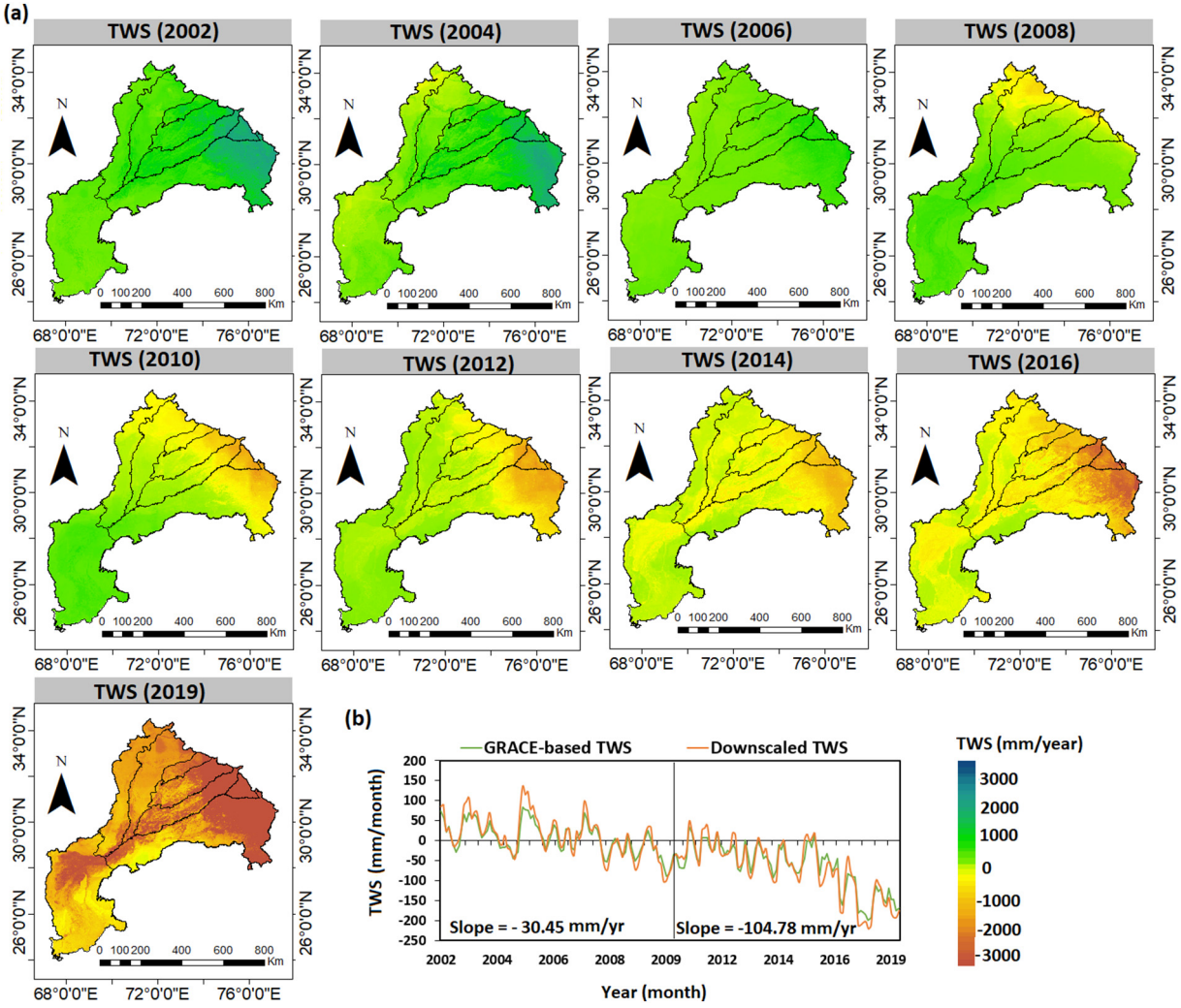


**Fig. 4.** a) Spatial and temporal distribution of downscaled TWS over the IIB; b) basin average monthly time-series changes in TWS from 2002 to 2019.

downscaled GWS data capture distributed variations within these irrigated plains with variable rates of groundwater depletion depending on cropping systems and other anthropogenic factors. This is a notable advancement in the characterization of distributed GWS variations within each irrigated plain compared to previous studies that investigated GWS variations using satellite observations with spatial resolutions ranging from $1^0$ to $0.25^0$ (Iqbal et al., 2016; Iqbal et al., 2017; Ali et al., 2021; Zhu et al., 2021; Akhter et al., 2021).

Fig. 6 presents the Sen's slope of GWS variations corresponding to different cropping systems (Fig. 6 a-b) and time series of changes in GWS for eight irrigated plains (Fig. 6 c-j) from 2002 to 2019. The GWS is declining over all the irrigated plains. A strong heterogeneity is observed in the GWS decline with the highest rate in the upstream regions such as BIST Doab and Delhi Doab where irrigated cotton-wheat and rice-wheat cropping systems are present (Fig. 6 a-b). The highest annual GWS decline was in Dehli Doab (−325.55 mm/year) followed by BIST Doab (−186.86 mm/year), BARI Doab (−119.20 mm/year) and RECHNA Doab (−100.82 mm/year) (Fig. 6 c-j). Other studies based on GRACE, Global Hydrological model (PCR-GLOBWB) and ground-based observations have also reported GWS decline in different periods ranging 41–45 mm/year during 2003–2008 (Rodell et al., 2009) and 46.3–68.0 mm/year from 2003 to 2013 (Prakash et al., 2014; Panda and Wahr, 2016; Long et al., 2016; Joshi et al., 2021). Our estimated mean annual GWS decline is relatively higher than previous reports between 2002 and 2014, because the GWS decline has become more abrupt since 2016 (Akhtar et al., 2022).

The GWS estimates obtained from the downscaled GRACE data provide reasonable resolution to understand variations at canal command scale. We investigated the GWS variations in 55 canal command areas, which have different water allocations and cropping systems (Fig. 7). While GWS has generally dropped from 2002 to 2019, hotspots of groundwater storage decline are more visible in the BARI Doab, Rachna Doab, and Delhi Doab canal command areas. The GWS decline is higher in the upper canal command areas as compared to those located in the lower Indus Basin (Fig. 7). This is likely because a higher percentage of irrigation demand in the upstream canal command areas is mainly supplied by groundwater and the consumptive fraction of irrigation withdrawal is larger (Biemans et al., 2016; Simons et al., 2020).

Downscaled GWS anomalies were validated using groundwater level data from 1489 observation wells in the study region, which were averaged at the corresponding 22 GRID cells of the GRACE data (see Fig. S10 in Supplementary Material). For instance, Fig. S10 shows the mean monthly time series of downscaled and observed GWS anomalies for GRID-1, GRID-4, GRID-7, GRID-9, GRID-11, GRID-14, GRID-17, GRID-19, GRID-21, and the average of all the grid cells. When compared to observational data, downscaled GWS agreed well with $R^2$ (0.67–0.81) and RMSE (49.70 mm/year – 116.17 mm/year). We obtained downscaled GWS estimates by subtraction of TWS data from GLDAS variables (SMS, CWS, and Qs). These components may cause uncertainty in GWS downscaling. Fig. S11 show the uncertainty in GWS associated with different error sources. Total uncertainty in GWS was estimated at 5.68 mm/month. While the individual

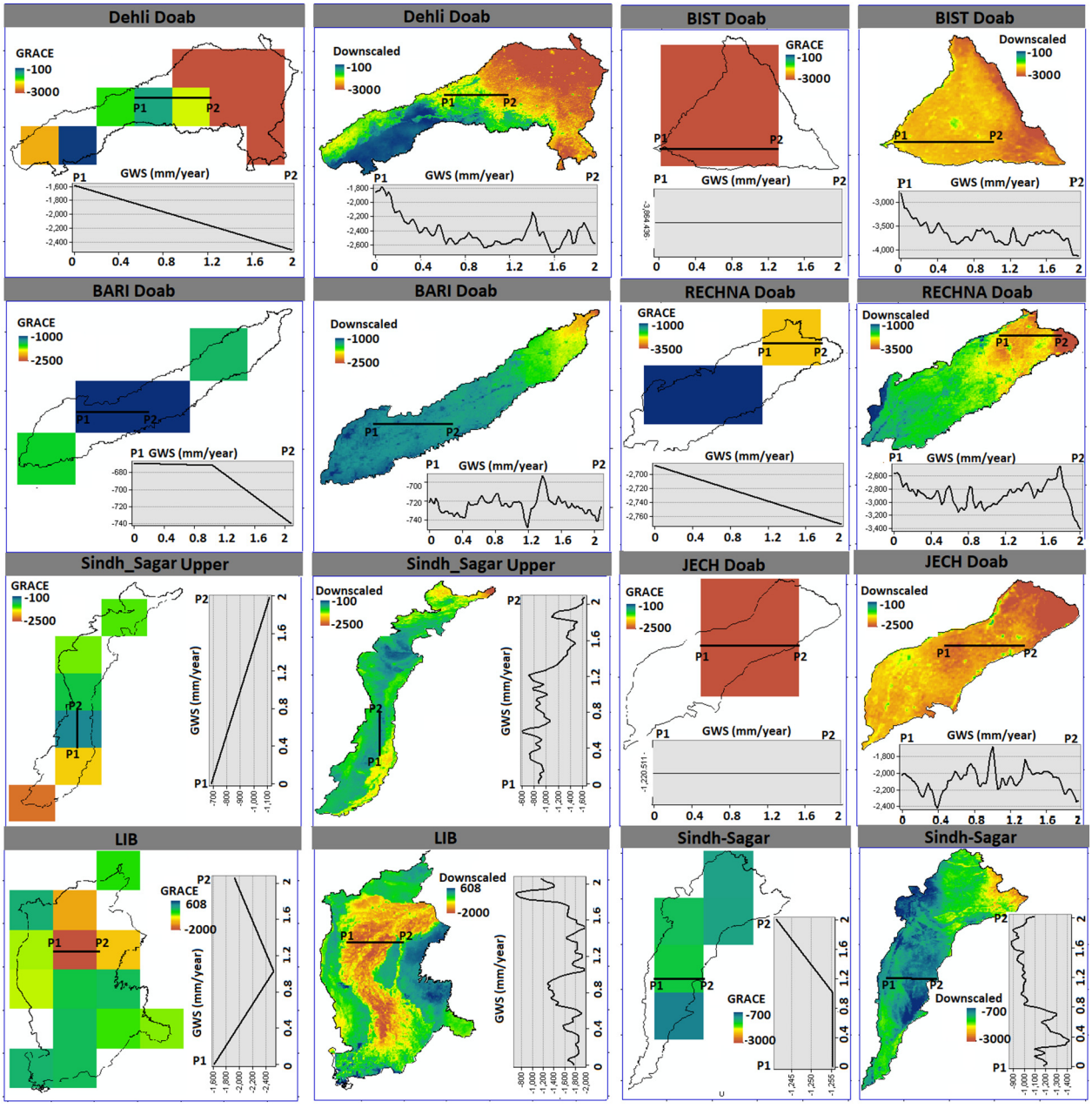


**Fig. 5.** Comparison of 1° × 1° GRACE-based GWS and downscaled GWS (1 km × 1 km) for different irrigated plains in the IIB for the year 2019. [1st and 3rd columns represent GRACE-based GWS, while 2nd and 4th columns represent downscaled GWS estimates].

uncertainties associated with downscaled TWS and GLDAS variables were 5.46 mm/month (TWS), 1.89 mm/month (SMS), 0.11 mm/month (Qs) and 0.01 mm/month (CWS).

### *4.4. How much groundwater has been depleted?*

GRACE data generally do not provide direct measurements of the amount of depletion; however, they provide estimates of water storage anomalies caused by anthropogenic activities (Felfelani et al., 2017; Huang et al., 2015). We estimated net groundwater depletion by combining GRACE-based downscaled GWS with SWAT model results and ground-based observational data, using a spatial water balance approach. A strong spatial heterogeneity in groundwater depletion is observed in the study area with relatively less depletion in the southern IIB (200–600 mm/year) and greater depletion in the northeast and central command areas (1100–1400 mm/year) (Fig. 8). The distributed groundwater depletion (DEPgw) increased continuously in different canal command areas during the 2002–2019 period (Fig. 8). For instance, net DEPgw in most canal command areas (e.g., BARI Doab, Rachna Doab, and Delhi Doab) ranged between 200 and 600 mm/year in 2002, which reached >1400 mm/year in 2019. This is consistent with the reported net groundwater depletion (800–1000 mm/year) in northeast and central canal command areas (Dehli, Indian Punjab and Pakistan Punjab) for year 2007 (Cheema et al., 2014).

Volumetric distribution of DEPgw was calculated individually for IIB's 55 canal command areas (See Fig. S12 in Supplementary Material). The rate of groundwater depletion is increasing in Delhi Doab and BIST Doab by 0.21–0.35 m/year while some canal command areas showed a decreasing trend by −0.036 m/year (Fig. S12a). Total loss of groundwater reserves over the 18-year period varies in the study area with the highest loss observed in Dehli Doab by >50 km$^3$ followed by 7.8–49 km$^3$ in the upstream (e.g., JECH, RACHNA Doabs), and 0.77–7.77 km$^3$ in the downstream canal

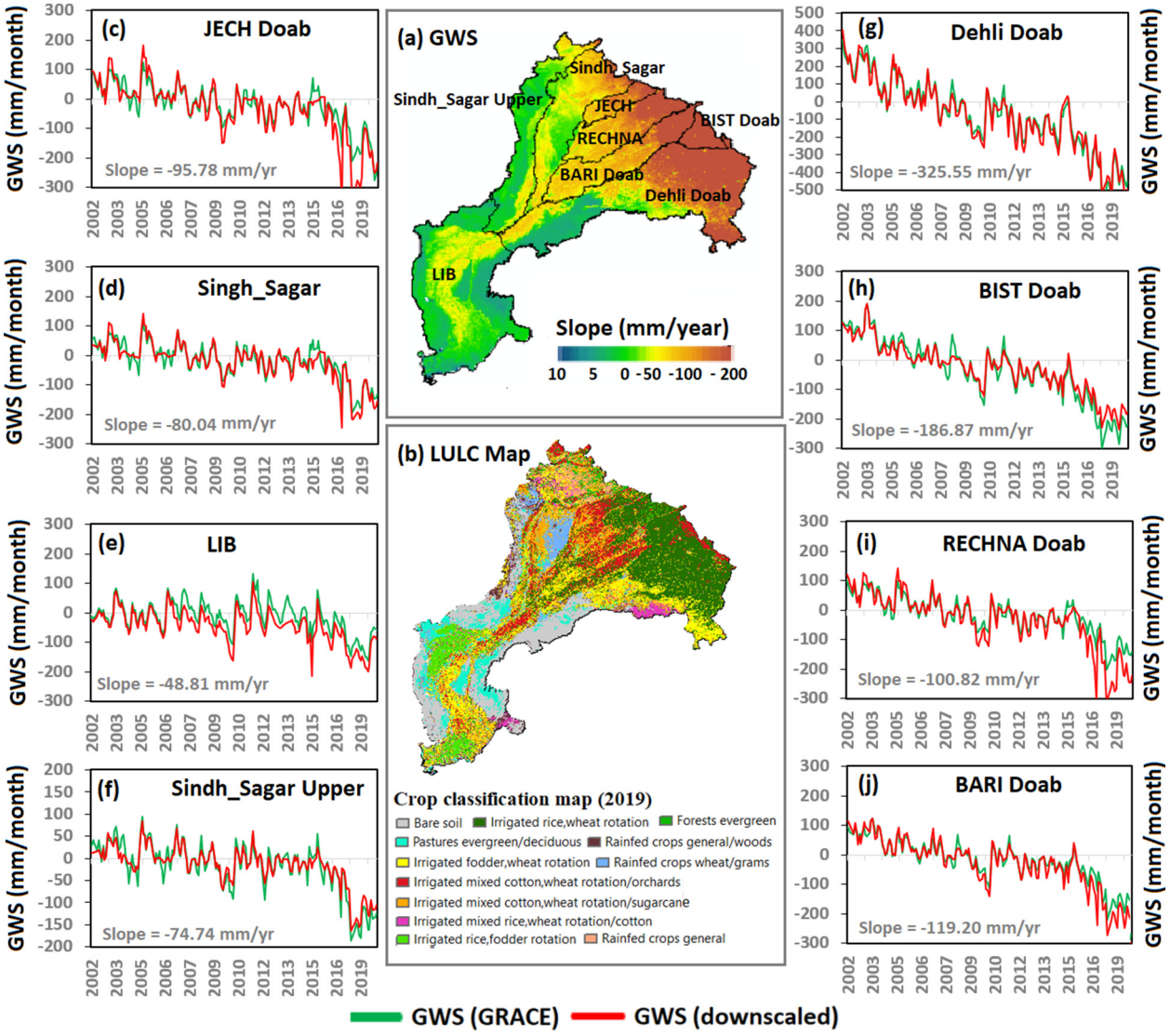


**Fig. 6.** (a-b) Spatial distribution of changing trend in GWS corresponding to different cropping systems and (c-j) GWS variations for the irrigated plains from 2002 to 2019.

command areas (Fig. 8b). Table 3 summarized the comparison of GRACE-based DEPgw estimates with observational data over selected GRIDs in the study region. The depletion rate and total groundwater loss calculated with downscaled GRACE data show similar changes over all GRIDs when compared with observational data. On average, total groundwater depletion was estimated to be −28.59 $km^3$ with downscaled GRACE and − 29.20 $km^3$ with observational data. An alarming rate of groundwater depletion (24–32 $km^3$) in the metropolitan region of Dehli has also been reported by Joshi et al. (2021). Iqbal et al. (2016) estimated mean groundwater depletion to be ~12 $km^3$ in the upstream irrigated regions of Punjab from 2003 to 2016. Ali et al. (2022) have reported Indus basin's average groundwater depletion to be 34.24–41.44 $km^3$ (with GRACE data), 43.28–49.14 $km^3$ (WGHM model), 43.28 $km^3$ (with PCR-GLOBWB) and 32.13 $Km^3$ (with observational data). Similar findings on groundwater over-exploitation have been reported for different regions of the Indus Basin (Iqbal et al., 2016; Rodell et al., 2009; IUCN, 2010; Ali et al., 2021; Roy et al., 2020).

### 4.5. What causes the decline in GWS and the increase in DEPgw?

Groundwater depletion variations in the IIB are associated with several drivers such as types of cropping systems, distribution of precipitation, surface water diversion and rainfall-induced recharge, and groundwater storage variations across the study region.

#### 4.5.1. Linkage between groundwater depletion and cropping systems

Detailed representation of seasonal cropping systems leads to more accurate estimation of the extent and timing of groundwater depletion. A variety of cropping systems with different water requirements exist in the IIB such as mixed cotton-wheat rotation/sugarcane, rice-fodder, fodder-wheat, rice-wheat, cotton, wheat rotation/orchards, and rice-wheat rotation (Table. 4 & Fig. 1). According to Cheema et al. (2014), number (depth) of irrigations in rice-wheat is 15 (100 mm) for rice and 4 (75 mm) for wheat, compared to cotton-wheat (5 (120 mm) for cotton and 4 (75 mm) for wheat)). Our results indicate that average groundwater depletion is higher (730.86 mm/year) in regions with rice-wheat cropping system where 1006.45 mm/year of groundwater is withdrawn for irrigation (Table. 4). The second highest depletion is detected in mixed cotton-wheat rotation (663 mm/year), where groundwater supply for irrigation is estimated to be 890.01 mm/year. Higher groundwater depletion in the BIST Doab and Delhi Doab is associated with rice-wheat production since the net amount of irrigation required is higher than other cropping systems (Arshad et al., 2019; Cheema et al., 2014). Muzammil et al. (2020) applied a spatio-temporal water footprint (WF) assessment technique, reporting that sugarcane, cotton, and rice are highly water-intensive, consuming 57% of the annual water use in the IIB. Fodder-wheat (Rabi cropping system) ranks third in water consumption, contributing to an annual groundwater depletion of 623.79 mm/year, nearly equal to cotton-wheat.

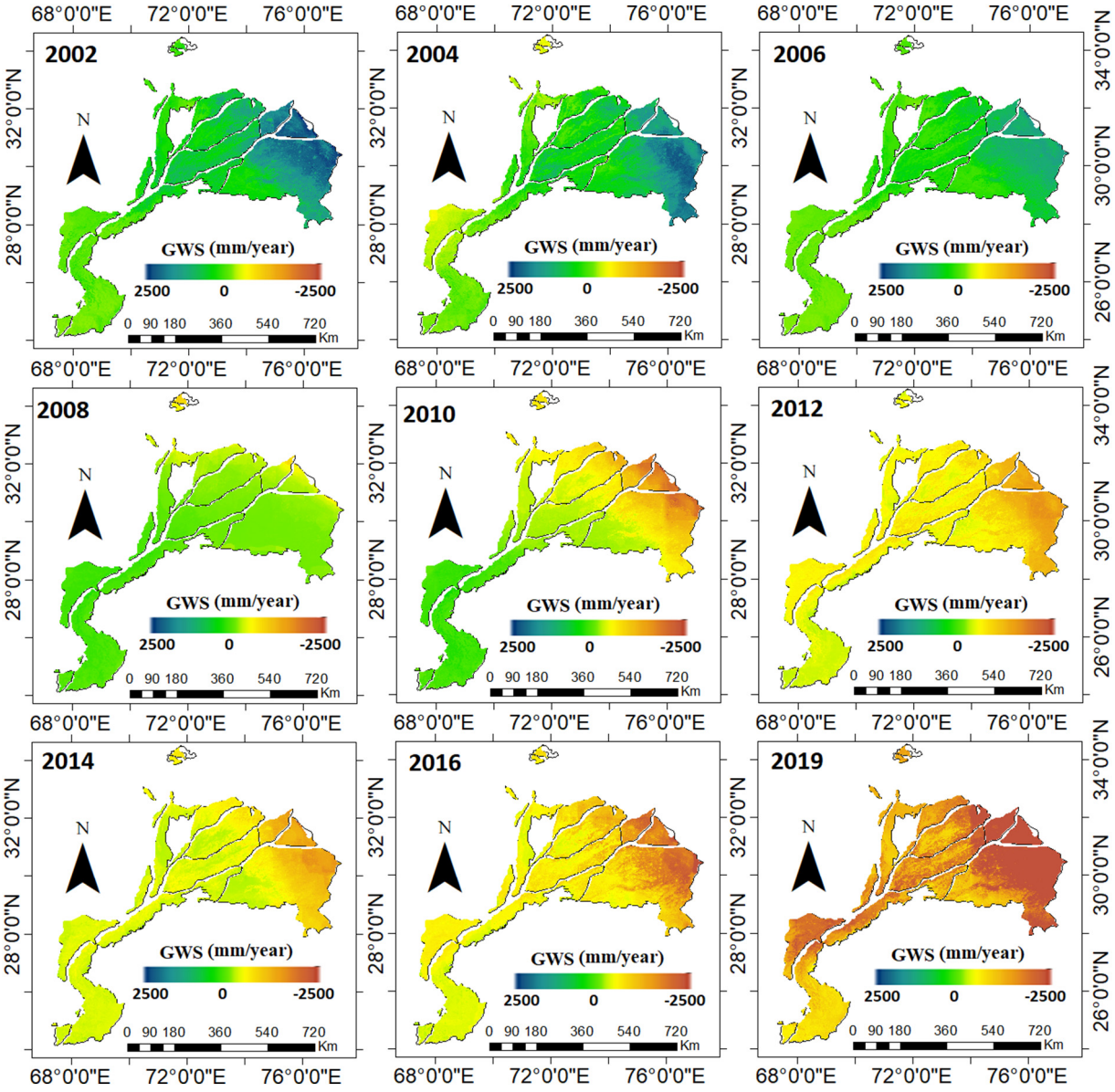


**Fig. 7.** Spatial-temporal variations in GWS estimated from downscaled GRACE data in different canal command areas during 2002–2019.

Groundwater use is generally higher during the Rabi season as compared to Kharif (Archer et al., 2010; Masih and Giordano, 2014; Kirby et al., 2017; Arshad et al., 2019). The total irrigated area used to grow major food crops in the Rabi cropping systems is greater than in the Kharif cropping systems, necessitating more water. In the winter, Rabi copping systems are irrigated primarily by groundwater, while melt runoff is the primary irrigation water source in the summer (Biemans et al., 2016).

*4.5.2. Increasing groundwater withdrawal for irrigation and grain production*

Increased pumping to meet the growing demands of grain production also contributes to the declining storage and increasing depletion of groundwater reserves. We compared the spatial-temporal patterns of GWS, $IRR_{total}$, $IRR_{gw}$, and $DEP_{gw}$ with crop production time series from the Pakistan Bureau of Statistics (https://www.pbs.gov.pk/) and Agricultural Statistics India (http://data.icrisat.org/dld/src/additional.html). While total irrigation water supplied from the aquifer increased continuously since 2002, reaching 2200 mm/year by 2019, strong spatial heterogeneity in changes of groundwater consumption exist across the study area (See Fig. S13 in Supplementary Material). For example, the increase in groundwater for irrigation was greater in the Delhi and BIST doabs whereas there was almost no change in the lower Indus Basin (Fig. S13). $IRR_{gw}$ in the upstream canal command areas is increasing by 16–110 mm/year (Fig. 9a) which is associated with an increase in grain sown area by 8.0–138 ha/year (Fig. 9b) and crop production by 50–729 ton/ha/year (Fig. 9c). The upstream canal command areas have a large proportion of wheat, rice, and cotton cropping systems (Arshad et al., 2019; Peña-Arancibia et al., 2021; Muzammil et al., 2021) which primarily use groundwater (Masih and Giordano, 2014; Biemans et al., 2016; Kirby et al., 2017; Arshad et al., 2019). The opposite trend is observed in the downstream regions where $IRR_{gw}$ is decreasing by (−5 to −38 mm/year) corresponding to a decline in crop sown area (−4.06–17.13 ha/year) and crop production (−31 to −148 ton/ha/year) (Fig. 9a-c). Peña-Arancibia et al. (2021) also reported an overall increase in irrigated area by 15% in the upper canal command areas located in Punjab Province and 13% decline in Sindh region from 1981 to 2013. We compiled times series data of crop production, groundwater storage, total irrigation, groundwater depletion variations from 2002 to 2019 for the eight irrigated plains (Fig. 9d-i). BIST Doab and Dehli Doab have the highest cropping area ($12{,}000 \times 10^3$ ha) while northeast (Sindh Saghar) and LIB have relatively lower cropping area ranging from $1800 \times 10^3$–$2700 \times 10^3$ ha. Crop sown area and production increased gradually from

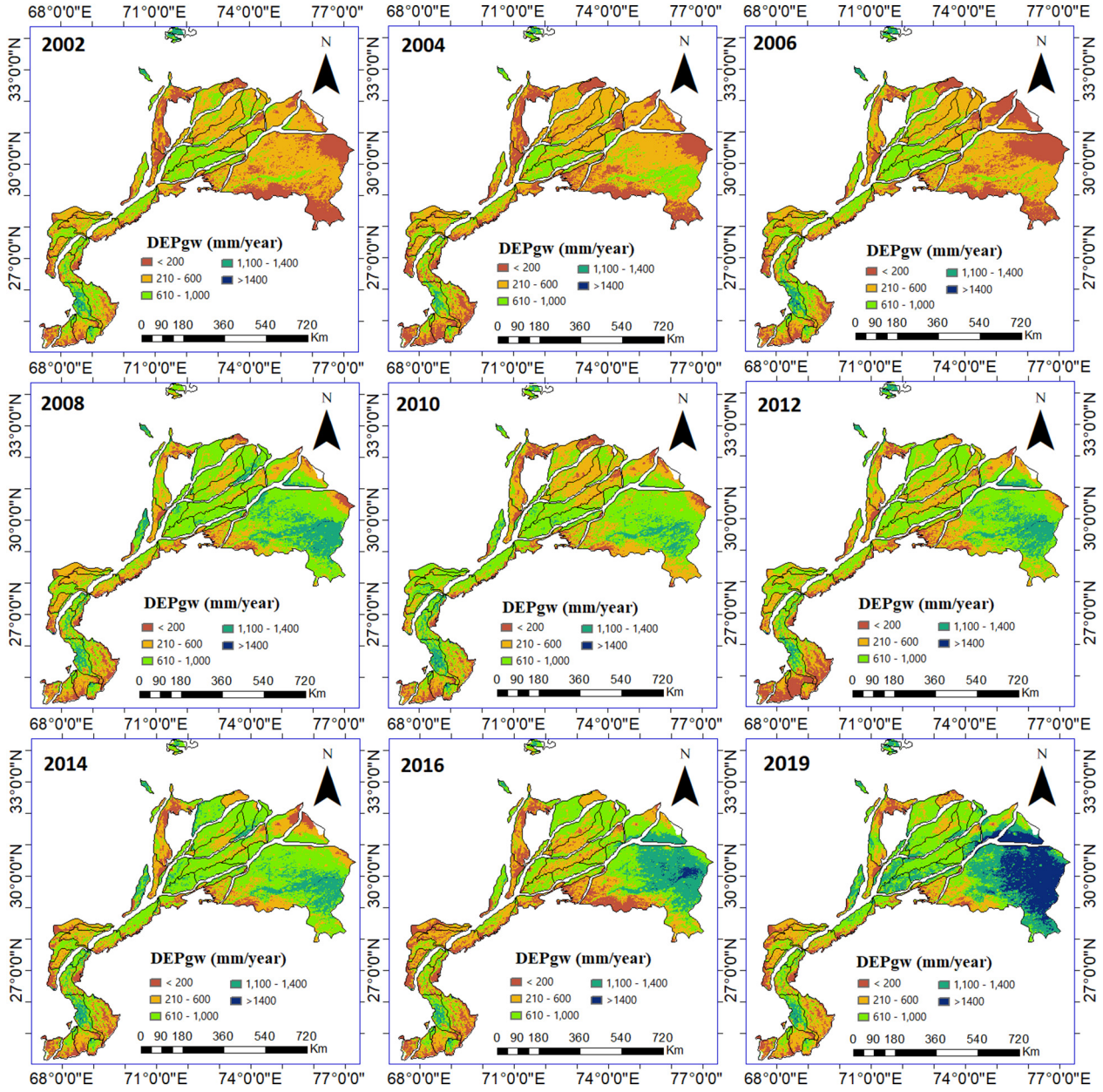


**Fig. 8.** DEPgw estimated by combining downscaled-GWS with SWAT results in different canal command areas during 2002–2019.

**Table 3**
Validation of GRACE-based DEPgw with observational data over selected grids (grid area: 12321 km$^2$) and average of 22 GRACE grids.

| Grid ID | Data type | Sen's slope (GWSA (mm/month)) | Depletion Rate (km$^3$/year) | Total DEPgw (km$^3$) |
|---|---|---|---|---|
| 1 | Observational | −13.08 | −1.93 | −32.87 |
| | GRACE-downscaled | −11.95 | −1.77 | −30.04 |
| 4 | Observational | −10.05 | −2.10 | −25.26 |
| | GRACE-downscaled | −8.81 | −1.85 | −22.15 |
| 17 | Observational | −24.02 | −3.55 | −60.36 |
| | GRACE-downscaled | −21.05 | −3.11 | −52.91 |
| 19 | Observational | −8.00 | −1.68 | −20.12 |
| | GRACE-downscaled | −8.65 | −1.81 | −21.75 |
| 21 | Observational | −10.55 | −2.21 | −26.52 |
| | GRACE-downscaled | −13.02 | −2.73 | −32.73 |
| Average (22 GRIDs) | Observational | −11.62 | −2.43 | −29.20 |
| | GRACE-downscaled | −11.38 | −2.38 | −28.59 |

**Table 4**
Average amount of groundwater storage changes, total irrigation, groundwater for irrigation, and groundwater depletion for different cropping systems from 2002 to 2019.

| Land use and cropping systems | GWS (mm/year) | IRR $_{total}$ (mm/year) | IRR $_{gw}$ (mm/year) | DEP $_{gw}$ (mm/year) |
|---|---|---|---|---|
| Rainfed crops general/woods | −152.2 | 698.53 | 236.25 | 136.47 |
| Irrigated mixed rice, wheat rotation/cotton | −804.8 | 871.54 | 531.38 | 423.56 |
| Rainfed crops wheat/grams | −510.9 | 609.07 | 185.49 | 67.51 |
| Irrigated fodder, wheat rotation | −842.7 | 1131.95 | 735.83 | 623.79 |
| Irrigated mixed cotton, wheat rotation/sugarcane | −637.7 | 1048.83 | 668.88 | 482.26 |
| Rainfed crops general | −735.7 | 1065.01 | 667.81 | 468.18 |
| Irrigated rice, fodder rotation | −626.8 | 1095.73 | 678.86 | 598.69 |
| Irrigated mixed cotton, wheat rotation/orchards | −751.4 | 1243.27 | 890.01 | 663.91 |
| Irrigated rice, wheat rotation | −1393.3 | 1288.31 | 1006.45 | 730.86 |

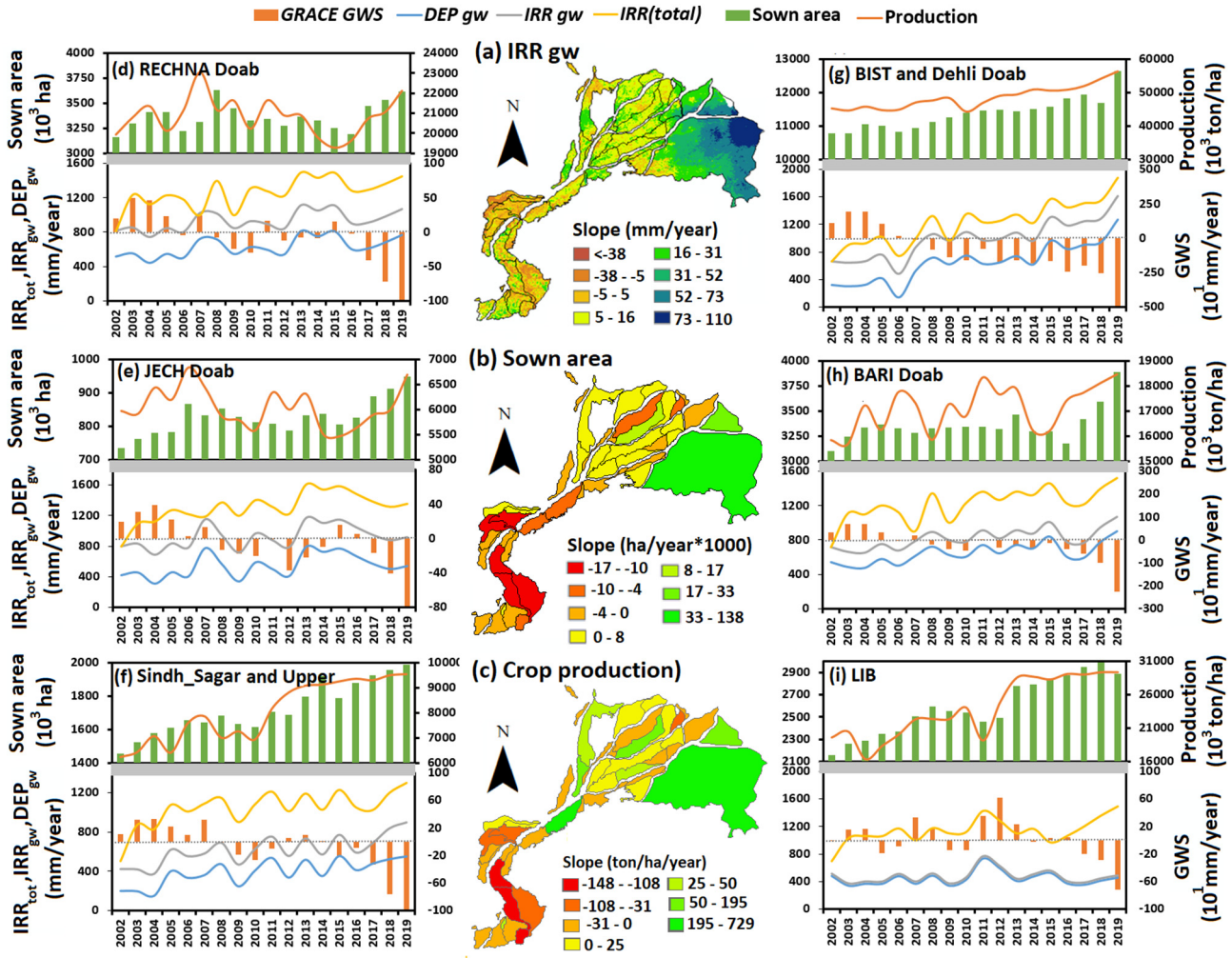


**Fig. 9.** (a-c) Spatial distribution of changing trend in groundwater irrigation ($IRR_{gw}$), crop sown area and production based on Sen's slope values from 2002 to 2019 over 55 canal command areas, and (d-i) time series variations in GWS, $IRR_{total}$, $IRR_{gw}$, and $DEP_{gw}$, crop sown area, and production from 2002 to 2019 over eight irrigated plains in the IIB.

2002 to 2019 for all irrigated plains except RECHNA Doab and JECH Doab, where it increased from 2002 to 2006 but then slowed significantly from 2006 to 2016. Overall, there is good agreement between year-to-year changes in IRRgw with the crop sown area and production, resulting in a clear change in GWS and DEPgw. For instance, IRRgw in Sindh-Sagar has increased from 400 mm/year (2002) to 800 mm/year (2019) and these changes correspond to increasing crop sown area from 1400 $\times$ $10^3$ ha (2002) to 2000 $\times$ $10^3$ ha (2019) (Fig. 9d-i). Table S2 shows that IRRgw, crop sown area, and production have negative correlation coefficients (CC at $p \leq 0.05$) with GWS, while the opposite correlation with DEPgw is seen on the majority of the IIB's irrigated plains. Overall, maximum positive correlation values of IRRgw, crop sown area, and production with DEPgw were found as 0.98, 0.89, 0.81, respectively over the BIST and RECHNA Doab indicating these drivers have significant impacts on the groundwater depletion (See Table S2 in Supplementary Material). Previous studies also reported that net crop irrigation requirement in the IIB has dramatically increased in recent decades which is associated with increasing crop sown area as well as climate warming leading to consuming more water (Arshad et al., 2019; Muzammil et al., 2020).

*4.5.3. Precipitation distribution and GWS changes*

The increase in evapotranspiration and decline in precipitation could contribute to falling groundwater levels in surrounding aquifers (Basharat et al., 2014; Ahmed and Wiese, 2019). The study region covers diverse climatic conditions where the precipitation distribution changes seasonally. Most of the precipitation occurs (66%–77%) during the summer season (JJAS) and a much lower proportion (16%–20%) in the winter season (JFMA) (Minallah and Ivanov, 2019). Fig. S14 shows the relationship between long-term average monthly precipitation and GWS changes across the study region. It is noteworthy that there is an agreement in precipitation seasonality and GWS changes. GWS experienced a larger negative anomaly in the dry season when precipitation amount was <20 mm/month. However, peak level of precipitation lags the peak level of GWS decline by approximately 2-months which is also reported by Akhtar et al. (2022).

*4.5.4. Surface water diversions and rainfall-induced recharge*

Surface water diversions are an important factor that controls groundwater storage and depletion variations in the IIB, which is the largest surface irrigation system in the world (Basharat et al., 2014; Basharat, 2019). The flow of eastern rivers in the IIB has gradually decreased since the Indus Waters Treaty (IWT) of 1960, necessitating more groundwater withdrawal to cope with the dwindling surface water (Indus Water Treaty (IWT), 1960; Basharat et al., 2014). The surface irrigation system in the IIB allocates water on a supply basis rather than based on demand. Since surface water supply is insufficient to sustain food production in some canal command areas, the growing area under cultivation has put a strain on available groundwater resources (Laghari et al., 2012). Table. 5 summarizes the canal-wise changes in GWS and depletion corresponding to average amount of rainfall-induced recharge and surface water diversions. Surface water diversion varies among the canal command areas. The rate of decline in GWS is higher in Dehli Doab (−351.04 mm/year) followed by BIST Doab (−341.40 mm/year), Upper Bari Canal (−198.48 mm/

**Table 5**
Changes in groundwater storage (GWS) and depletion ($DEP_{gw}$) corresponding to rainfall-induced recharge ($GW_{rech}$) and surface water diversions (CWS).

| Canal Command Area | GWS (Sen's slope: mm/yr) | DEPgw (Sen's slope: mm/yr) | $GW_{rech}$ (mm/yr) | CWS (mm/yr) |
|---|---|---|---|---|
| Upper Swat Canal | 25.61 | 5.79 | 986.38 | 200.00 |
| Lower Swat (& Doaba Sholgara Canal) | 35.83 | 0.51 | 986.38 | 180.00 |
| Kabul River (Jui Shaikh & Inundation) | 36.32 | −0.75 | 986.38 | 200.00 |
| Warsak High Level Canal (Left Bank) | 34.98 | 7.34 | 986.38 | 180.00 |
| Warsak High Level Canal (Left Bank) | 28.90 | 3.97 | 986.38 | 200.00 |
| Bannu Scarp | 16.03 | 2.52 | 820.46 | 170.00 |
| Thal Canal | −47.49 | 9.38 | 247.30 | 325.00 |
| Upper Jehlum Canal | −55.11 | 12.42 | 358.56 | 720.00 |
| Lower Jehlum Canal | −31.55 | 13.94 | 374.97 | 300.00 |
| CRBC/Paharpur Canal | −5.90 | 1.53 | 190.40 | 200.00 |
| Marala Ravi Canal | −127.73 | 21.78 | 531.27 | 180.00 |
| Upper Chenab Canal | −50.60 | 10.30 | 369.96 | 325.00 |
| Jhang | −54.44 | 11.76 | 289.72 | 400.00 |
| Raya Branch (BRBD Inetranl) | −92.56 | 16.77 | 561.51 | 250.00 |
| Gugera | −69.77 | 12.29 | 188.53 | 430.00 |
| Central Bari Doab Canal | −166.53 | 23.17 | 207.35 | 400.00 |
| Lower Bari Doab Canal | −63.88 | 11.66 | 127.84 | 500.00 |
| Rangpur Canal | −95.91 | 12.84 | 175.39 | 500.00 |
| Upper Dipalpur Canal | −154.06 | 23.06 | 153.56 | 250.00 |
| Haveli Canal | −88.75 | 15.52 | 103.44 | 700.00 |
| Lower Dipalpur Canal | −49.74 | 11.39 | 114.61 | 530.00 |
| Muzffgarh Canal | −77.58 | 10.34 | 104.08 | 900.00 |
| Sidhnai Canal | −61.17 | 9.25 | 110.43 | 500.00 |
| Pakpattan Canal | −52.40 | 9.69 | 109.81 | 450.00 |
| Dera Ghazi Khan Canal | −75.58 | 14.46 | 227.56 | 800.00 |
| Fordwah | −44.71 | 15.31 | 120.78 | 400.00 |
| Sadiqia Canal | −3.05 | 16.19 | 134.75 | 545.00 |
| Mailsi Canal (Lower Mailsi + Lower Pakpa) | −56.55 | 12.89 | 111.92 | 550.00 |
| Sadiqia Canal | −37.85 | 6.64 | 60.24 | 630.00 |
| Upper Bahawal & Qaim Canal | −28.12 | 10.75 | 107.99 | 900.00 |
| Bahawal Canal | −61.03 | 15.81 | 57.47 | 640.00 |
| Abbasia Canal | −68.06 | 18.02 | 42.52 | 300.00 |
| Panjnad Canal | −42.14 | 6.83 | 30.40 | 600.00 |
| Pat feeder | 5.55 | −5.71 | 13.09 | 800.00 |
| Desert Canal | 0.90 | 0.11 | 13.32 | 740.00 |
| Begari Canal | 0.57 | −0.78 | 13.41 | 700.00 |
| Ghotki Canal | −3.17 | 3.10 | 28.62 | 700.00 |
| North West Canal | 5.94 | −4.00 | 13.28 | 550.00 |
| Rice Canal | 6.47 | 0.65 | 13.09 | 900.00 |
| Khairpur West Canal | 0.02 | 5.11 | 18.22 | 630.00 |
| Dadu Canal | 8.27 | 2.58 | 13.57 | 630.00 |
| Khairpur East Canal | 0.41 | 1.23 | 58.49 | 440.00 |
| Rohri (North) Canal | 3.75 | 7.48 | 45.75 | 530.00 |
| Nara Canal | −38.84 | 0.26 | 58.87 | 700.00 |
| Rohri (south) Canal | −17.18 | 3.58 | 54.18 | 530.00 |
| Lake | −36.24 | 1.29 | 24.51 | 200.00 |
| Fuleli Canal | −55.86 | 7.65 | 38.43 | 900.00 |
| Pinyari Canal | −67.87 | 10.87 | 28.84 | 630.00 |
| Gaja Branch (Old Fuleli/Lined Canal) | −40.56 | 1.17 | 29.33 | 630.00 |
| Lake | −35.97 | 5.94 | 24.51 | 500.00 |
| Kalri Canal | −51.83 | 8.47 | 24.51 | 750.00 |
| Lined Canal (Tando Bago) | −73.38 | 0.91 | 49.06 | 500.00 |
| Upper Bari | −198.48 | 29.03 | 329.31 | 330.00 |
| BIST Doab | −341.40 | 53.03 | 439.79 | 150.00 |
| Dehli Doab | −351.04 | 50.24 | 279.04 | 320.00 |

year), and Central Bari Doab Canal (−166.53 mm/year). These rates correspond to rainfall-induced recharge (canal water) of 279 mm/year (320 mm/year), 439.79 mm/year (150 mm/year), 329.31 mm/year (330 mm/year), 207.35 mm/year (400 mm/year). Overall, canal command areas with reduced surface water diversions experienced larger decline in groundwater storage (Table. 5). Due to low rainfall (Ahmad et al., 2014) and low flows from Ravi and Sutlej rivers, the groundwater recharge is insufficient to prevent a decline in groundwater storage in these regions (Basharat and Tariq, 2013). The fluctuation of surface water (high flow in the summer and low flow in the winter) (Dahri et al., 2021; Smolenaars et al., 2021), results in an uncertain yield. By contrast, groundwater is available on demand throughout the year, increasing the reliability of crop production (Biemans et al., 2016). It is worth noting that some upstream canal command areas (e.g., Upper Swat, Lower Swat, Warsak high-level canal) that receive less surface water from canal diversions experience no groundwater decline due to rainfed agriculture (Table. 5), and meanwhile the rainfall-induced recharge from monsoons helps to replenish the groundwater reserves (Qureshi and Perry, 2021; Khan et al., 2021). Gradually increasing water consumption in the upper Indus basin is reducing dry season surface water availability (Smolenaars et al., 2021), thus increasing the reliance on groundwater in the lower Indus Basin (Ali et al., 2021).

### *4.6. Limitations and future directions*

The contributions of our study should be considered in light of the following limitations, which can be addressed by future investigations to further improve the capability to detect groundwater depletion hotspots. First, the SWAT modeling component of the framework focused on matching the total amount of irrigation water used in the simulation to the total reported irrigation from surface water and groundwater in the study area. Although this approach accounts for the distribution of surface water allocation in the IIB, the SWAT model can be improved by explicit modeling of surface water diversions through the network of water conveyance infrastructure. Second, we only downscaled GRACE Level-3 Spherical Harmonic (SH) solution. The analysis can be expanded to compare the consistency of the detected groundwater depletion hotspots by downscaling other Mascon products, which are available at $0.5^0$ to $0.25^0$. Third, limited groundwater level observations across the entire IIB poses a challenge for a comprehensive process of validation. However, the estimated groundwater depletion matches the estimates based on the available observational groundwater level data. Likewise, our estimates are comparable with the reported values in the published literature. Finally, detailed investigation of crop production footprints on the groundwater system in the IIB can be performed using empirical relations and data driven approaches to cross-examine our findings.

## 5. Conclusions

High-resolution GRACE-based GWS integrated with SWAT results advance the ability to strategically detect the hotspots of groundwater storage variation and depletion within each irrigated plain with different cropping systems in the IIB. The GWS changes exhibit significant spatial heterogeneity, with the greatest decline occurring in upstream regions such as BIST Doab and Delhi Doab, although a slight decline is also observed in the lower Indus Basin. Groundwater depletions were higher in the plains with irrigated rice-wheat and cotton-wheat cropping systems. Our results revealed that temporal and spatial heterogeneity of GWS and DEPgw changes are strongly associated with the distribution of surface water allocation, types of cropping systems, and growing crop production in different canal command areas. In general, irrigated plains that have low flows and receive less precipitation are showing large groundwater abstraction and decline in groundwater storage. Further, an increasing pattern of IRRgw is consistent with increased crop sown area and production, resulting in a clear change in GWS and DEPgw. Uncontrolled groundwater abstraction consistently in excess of recharge is exacerbating groundwater stress, which in turn threatens the sustainability of groundwater reserves in the IIB.

## CRediT authorship contribution statement

**Arfan Arshad** conceived of the ideas, performed the experiments, analyzed the results, and prepared the first draft of the manuscript under the supervision of **Ali Mirchi**. **Maryam Samimi and Bashir Ahmad** provided oversight and helped with technical review and editing the manuscript.

## Declaration of competing interest

The authors declare that they have no known competing financial interests or personal relationships that could have appeared to influence the work reported in this paper.

## Acknowledgement

The first author acknowledges the US-PAK Knowledge Corridor Funding provided by Higher Education Commission (HEC), Pakistan. The second author acknowledges funding from the National Science Foundation (NSF Award 2114701) of the United States. We thank the Pakistan Meteorological Department (PMD) and Punjab Irrigation Department (PID) for providing the datasets for this study. We appreciate insightful comments from four anonymous reviewers. Any opinions, findings, conclusions, or recommendations expressed in this publication are solely those of the authors.

## Appendix A. Supplementary data

Supplementary data to this article can be found online at https://doi.org/10.1016/j.scitotenv.2022.156044.

## References

Ahamed, A., Knight, R., Alam, S., Pauloo, R., Melton, F., 2022. Assessing the utility of remote sensing data to accurately estimate changes in groundwater storage. Sci. Total Environ. 807, 150635.

Ahamed, A., Knight, R., Alam, S., Pauloo, R., Melton, F., 2022. Assessing the utility of remote sensing data to accurately estimate changes in groundwater storage. Sci.Total Environ. 807, 150635.

Ahmad, S., 2009. Water availability in Pakistan: Paper presented by Dr. Shahid Ahmad, Member PARC. National Seminar on "Water Conservation, Present Situation and Future Strategy, p. 114.

Ahmad, W., Fatima, A., Awan, U.K., Anwar, A., 2014. Analysis of long term meteorological trends in the middle and lower Indus Basin of Pakistan—a non-parametric statistical approach. Glob. Planet. Chang. 122, 282–291.

Ahmed, M., 2020. Sustainable management scenarios for northern Africa's fossil aquifer systems. J. Hydrol. 589, 125196.

Ahmed, M., Abdelmohsen, K., 2018. Quantifying modern recharge and depletion rates of the Nubian Aquifer in Egypt. Surv. Geophys. 39 (4), 729–751.

Ahmed, M., Wiese, D.N., 2019. Short-term trends in Africa's freshwater resources: rates and drivers. Sci. Total Environ. 695, 133843.

Ahmed, M., Sultan, M., Wahr, J., Yan, E., 2014. The use of GRACE data to monitor natural and anthropogenic induced variations in water availability across Africa. Earth Sci. Rev. 136, 289–300.

Ahmed, M., Aqnouy, M., El Messari, J.S., 2021. Sustainability of Morocco's groundwater resources in response to natural and anthropogenic forces. J. Hydrol. 603, 126866.

Akhtar, F., Nawaz, R.A., Hafeez, M., Awan, U.K., Borgemeister, C., Tischbein, B., 2022. Evaluation of GRACE derived groundwater storage changes in different agro-ecological zones of the Indus Basin. J. Hydrol. 605, 127369.

Akhter, G., Ge, Y., Iqbal, N., Shang, Y., Hasan, M., 2021. Appraisal of remote sensing technology for groundwater resource management perspective in Indus Basin. Sustainability 13 (17), 9686.

Ali, S., Liu, D., Fu, Q., Cheema, M.J.M., Pham, Q.B., Rahaman, M., Dang, T.D., Anh, D.T., 2021. Improving the resolution of GRACE data for spatio-temporal groundwater storage assessment. Remote Sens. 13 (17), 3513.

Ali, S., Wang, Q., Liu, D., Fu, Q., Rahaman, M.M., Faiz, M.A., Cheema, M.J.M., 2022. Estimation of spatio-temporal groundwater storage variations in the Lower Transboundary Indus Basin using GRACE satellite. J. Hydrol. 605, 127315.

An, L., Wang, J., Huang, J., Pokhrel, Y., Hugonnet, R., Wada, Y., Cáceres, D., Müller Schmied, H., Song, C., Berthier, E., Yu, H., 2021. Divergent causes of terrestrial water storage decline between drylands and humid regions globally. Geophys. Res. Lett. 48 (23) p. e2021GL095035.

Archer, D.R., Forsythe, N., Fowler, H.J., Shah, S.M., 2010. Sustainability of water resources management in the Indus Basin under changing climatic and socio economic conditions. Hydrol. Earth Syst. Sci. 14 (8), 1669–1680.

Arnold, J.G., Srinivasan, R., Muttiah, R.S., Williams, J.R., 1998. Large area hydrologic modeling and assessment part I: model development 1. J.Am.Water Resour.Assoc. 34 (1), 73–89.

Arshad, A., Zhang, Z., Zhang, W., Gujree, I., 2019. Long-term perspective changes in crop irrigation requirement caused by climate and agriculture land use changes in Rechna Doab, Pakistan. Water 11 (8), 1567.

Arshad, A., Zhang, Z., Zhang, W., Dilawar, A., 2020. Mapping favorable groundwater potential recharge zones using a GIS-based analytical hierarchical process and probability frequency ratio model: a case study from an agro-urban region of Pakistan. Geosci. Front. 11 (5), 1805–1819.

Arshad, A., Zhang, W., Zhang, Z., Wang, S., Zhang, B., Cheema, M.J.M., Shalamzari, M.J., 2021. Reconstructing high-resolution gridded precipitation data using an improved downscaling approach over the high-altitude mountain regions of the Upper Indus Basin (UIB). Sci. Total Environ. 784, 147140.

Arshad, M., Ahmed, N., Cheema, J.M., 2008. Modeling approach for the assessment of recharge contribution to groundwater from surface irrigation conveyance system. Irrig. Drain. Syst. 22 (1), 67–77.

Awan, U.K., Ismaeel, A., 2014. A new technique to map groundwater recharge in irrigated areas using a SWAT model under changing climate. J. Hydrol. 519, 1368–1382.

Awan, U.K., Liaqat, U.W., Choi, M., Ismaeel, A., 2016. A SWAT modeling approach to assess the impact of climate change on consumptive water use in Lower Chenab Canal area of Indus basin. Hydrol. Res. 47 (5), 1025–1037.

Basharat, M., 2019. Water management in the Indus Basin in Pakistan: challenges and opportunities. Indus River Basin. Elsevier, pp. 375–388.

Basharat, M., Tariq, A.U.R., 2013. Long-term groundwater quality and saline intrusion assessment in an irrigated environment: a case study of the aquifer under the lbdc irrigation system. Irrig. Drain. 62 (4), 510–523.

Basharat, M., Umair Ali, S., Azhar, A.H., 2014. Spatial variation in irrigation demand and supply across canal commands in Punjab: a real integrated water resources management challenge. Water Policy 16 (2), 397–421.

Becker, R., Koppa, A., Schulz, S., Usman, M., aus der Beek, T., Schueth, C., 2019. Spatially distributed model calibration of a highly managed hydrological system using remote sensing-derived ET data. J. Hydrol. 577, 123944.

Bennett, G.D., 1967. Analysis of Aquifer Tests in the Punjab Region of West Pakistan. US Government Printing Office.

Biancamaria, S., Mballo, M., Le Moigne, P., Pérez, J.M.S., Espitalier-Noël, G., Grusson, Y., Cakir, R., Häfliger, V., Barathieu, F., Trasmonte, M., Boone, A., 2019. Total water storage variability from GRACE mission and hydrological models for a 50,000 km2 temperate watershed: the Garonne River basin (France). J.Hydrol.Reg.Stud. 24, 100609.

Biemans, H., Siderius, C., Mishra, A., Ahmad, B., 2016. Crop-specific seasonal estimates of irrigation-water demand in South Asia. Hydrol. Earth Syst. Sci. 20 (5), 1971–1982.

Bierkens, M.F., Wada, Y., 2019. Non-renewable groundwater use and groundwater depletion: a review. Environ. Res. Lett. 14 (6), 063002.

Castellazzi, P., Longuevergne, L., Martel, R., Rivera, A., Brouard, C., Chaussard, E., 2018. Quantitative mapping of groundwater depletion at the water management scale using a combined GRACE/InSAR approach. Remote Sens. Environ. 205, 408–418.

Chao, L., Zhang, K., Li, Z., Zhu, Y., Wang, J., Yu, Z., 2018. Geographically weighted regression based methods for merging satellite and gauge precipitation. J. Hydrol. 558, 275–289.

Cheema, M.J.M., Bastiaanssen, W.G., 2010. Land use and land cover classification in the irrigated Indus Basin using growth phenology information from satellite data to support water management analysis. Agric. Water Manag. 97 (10), 1541–1552.

Cheema, M.J.M., Immerzeel, W.W., Bastiaanssen, W.G.M., 2014. Spatial quantification of groundwater abstraction in the irrigated Indus basin. Groundwater 52 (1), 25–36.

Chen, J., Famigliett, J.S., Scanlon, B.R., Rodell, M., 2016. Groundwater storage changes: Present status from GRACE observations. Surv. Geophys. 37, 397–417. https://doi.org/10.1007/s10712-015-9332-4.

Chen, H., Zhang, W., Nie, N., Guo, Y., 2019. Long-term groundwater storage variations estimated in the Songhua River Basin by using GRACE products, land surface models, and in-situ observations. Sci. Total Environ. 649, 372–387.

Chen, L., He, Q., Liu, K., Li, J., Jing, C., 2019. Downscaling of GRACE-derived groundwater storage based on the random forest model. Remote Sens. 11 (24), 2979.

Chen, Z., Zheng, W., Yin, W., Li, X., Zhang, G., Zhang, J., 2021. Improving the spatial resolution of GRACE-derived terrestrial water storage changes in small areas using the machine learning spatial downscaling method. Remote Sens. 13 (23), 4760.

Dahri, Z.H., Ludwig, F., Moors, E., Ahmad, S., Ahmad, B., Ahmad, S., Riaz, M., Kabat, P., 2021. Climate change and hydrological regime of the high-altitude Indus basin under extreme climate scenarios. Sci. Total Environ. 768, 144467.

Dakhlalla, A.O., Parajuli, P.B., Ouyang, Y., Schmitz, D.W., 2016. Evaluating the impacts of crop rotations on groundwater storage and recharge in an agricultural watershed. Agric. Water Manag. 163, 332–343.

Duan, S.B., Li, Z.L., 2016. Spatial downscaling of MODIS land surface temperatures using geographically weighted regression: case study in northern China. IEEE Trans. Geosci. Remote Sens. 54 (11), 6458–6469.

Faber, N.K.M., 2002. Uncertainty estimation for multivariate regression coefficients. Chemom. Intell. Lab. Syst. 64 (2), 169–179.

Felfelani, F., Wada, Y., Longuevergne, L., Pokhrel, Y.N., 2017. Natural and human-induced terrestrial water storage change: a global analysis using hydrological models and GRACE. J. Hydrol. 553, 105–118.

Feng, W., Zhong, M., Lemoine, J.M., Biancale, R., Hsu, H.T., Xia, J., 2013. Evaluation of groundwater depletion in North China using the Gravity Recovery and Climate Experiment (GRACE) and ground-based measurements. AprilEGU General Assembly Conference Abstracts (pp. EGU2013-1796).

Gao, J., Li, S., 2011. Detecting spatially non-stationary and scale-dependent relationships between urban landscape fragmentation and related factors using geographically weighted regression. Appl. Geogr. 31, 292–302.

Gemitzi, A., Koutsias, N., Lakshmi, V., 2021. A spatial downscaling methodology for GRACE Total water storage anomalies using GPM IMERG precipitation estimates. Remote Sens. 13 (24), 5149.

Gumma, M.K., Thenkabail, P.S., Teluguntla, P., Whitbread, A.M., 2019. Indo-Ganges river basin land use/land cover (LULC) and irrigated area mapping. Indus River Basin. Elsevier, pp. 203–228.

Hassan, A., Jin, S., 2016. Water storage changes and balances in Africa observed by GRACE and hydrologic models. GeodesyGeodyn. 7 (1), 39–49.

Hu, K.X., Awange, J.L., Kuhn, M., 2022. Testing a knowledge-based approach for inferring spatio-temporal characteristics of groundwater in the Australian State of Victoria. Sci. Total Environ. 153113.

Huang, Y., Salama, M.S., Krol, M.S., Su, Z., Hoekstra, A.Y., Zeng, Y., Zhou, Y., 2015. Estimation of human-induced changes in terrestrial water storage through integration of GRACE satellite detection and hydrological modeling: a case study of the Y angtze R iver basin. Water Resour. Res. 51 (10), 8494–8516.
Hussain, D., Kao, H.C., Khan, A.A., Lan, W.H., Imani, M., Lee, C.M., Kuo, C.Y., 2020. Spatial and temporal variations of terrestrial water storage in upper Indus basin using GRACE and altimetry data. IEEE Access 8, 65327–65339.
Immerzeel, W.A., Droogers, P., 2008. Calibration of a distributed hydrological model based on satellite evapotranspiration. J. Hydrol. 349 (3-4), 411–424.
Immerzeel, W.W., Van Beek, L.P., Bierkens, M.F., 2010. Climate change will affect the Asian water towers. Science 328 (5984), 1382–1385.
Indus Water Treaty (IWT), 1960. Site Resources. World Bank, pp. 1–24.
Iqbal, N., Hossain, F., Lee, H., Akhter, G., 2016. Satellite gravimetric estimation of groundwater storage variations over Indus Basin in Pakistan. IEEE J.Sel.Top.Appl.Earth Obs.Remote Sens. 9 (8), 3524–3534.
Iqbal, N., Hossain, F., Lee, H., Akhter, G., 2017. Integrated groundwater resource management in Indus Basin using satellite gravimetry and physical modeling tools. Environ. Monit. Assess. 189 (3), 1–16.
IUCN, 2010. Beyond Indus Water Treaty: Ground Water And Environmental Management Policy Issues And Options. IUCN, Karachi, Pakistan.
Janjua, S., Hassan, I., Muhammad, S., Ahmed, S., Ahmed, A., 2021. Water management in Pakistan's Indus Basin: challenges and opportunities. Water Policy 23 (6), 1329–1343.
Jing, W., Yang, Y., Yue, X., Zhao, X., 2016. A comparison of different regression algorithms for downscaling monthly satellite-based precipitation over North China. Remote Sens. 8, 835.
Joshi, S.K., Gupta, S., Sinha, R., Densmore, A.L., Rai, S.P., Shekhar, S., Mason, P.J., van Dijk, W.M., 2021. Strongly heterogeneous patterns of groundwater depletion in Northwestern India. J. Hydrol. 598, 126492.
Khan, F.Y., Ashraf, A., Akhter, G., Baig, M.A., Baig, S.A., 2021. Appraisal of groundwater recharge in Neelum watershed (Upper Indus Basin) using geospatial water balance technique. Sci. Total Environ. 785, 147318.
Khan, M., Khan, W., 2020. Socioeconomic and recharge effect on spatial changes in the groundwater chemistry of Punjab, Pakistan: a multivariate statistical approach. SN Appl.Sci. 2 (8), 1–19.
Kirby, M., Mainuddin, M., Khaliq, T., Cheema, M.J.M., 2017. Agricultural production, water use and food availability in Pakistan: historical trends, and projections to 2050. Agric. Water Manag. 179, 34–46.
Laghari, A.N., Vanham, D., Rauch, W., 2012. The Indus basin in the framework of current and future water resources management. Hydrol. Earth Syst. Sci. 16 (4), 1063–1083.
Landerer, F.W., Swenson, S.C., 2012. Accuracy of scaled GRACE terrestrial water storage estimates. Water Resour. Res. 48 (4).
Li, Q., Liu, X., Zhong, Y., Wang, M., Zhu, S., 2021. Estimation of terrestrial water storage changes at small basin scales based on multi-source data. Remote Sens. 13 (16), 3304.
Liu, W., Bailey, R.T., Andersen, H.E., Jeppesen, E., Park, S., Thodsen, H., Nielsen, A., Molina-Navarro, E., Trolle, D., 2020. Assessing the impacts of groundwater abstractions on flow regime and stream biota: combining SWAT-MODFLOW with flow-biota empirical models. Sci. Total Environ. 706, 135702.
Liu, Z., Liu, Y., Wang, S., Yang, X., Wang, L., Baig, M.H.A., Chi, W., Wang, Z., 2018. Evaluation of spatial and temporal performances of ERA-interim precipitation and temperature in mainland China. J. Clim. 31 (11), 4347–4365.
Long, D., Yang, Y., Wada, Y., Hong, Y., Liang, W., Chen, Y., 2015. Deriving scaling factors using a global hydrological model to restore GRACE total water storage changes for China's Yangtze River Basin. Remote Sens. Environ. 168, 177–193.
Long, D., Chen, X., Scanlon, B.R., Wada, Y., Hong, Y., Singh, V.P., Chen, Y., Wang, C., Han, Z., Yang, W., 2016. Have GRACE satellites overestimated groundwater depletion in the Northwest India Aquifer? Sci. Rep. 6 (1), 1–11.
Masih, Ilyas, Giordano, Mark, 2014. Constraints and opportunities for water savings and increasing productivity through Resource Conservation Technologies in Pakistan. Agric. Ecosyst. Environ. 187, 106–115.
Masud, Muhammad Jehanzeb, Bastiaanssen, Wim G.M., 2017. Remote sensing and GIS applications in water resources management. Water Resour. Manag. 351–373.
Mehrnegar, N., Jones, O., Singer, M.B., Schumacher, M., Jagdhuber, T., Scanlon, B.R., Rateb, A., Forootan, E., 2021. Exploring groundwater and soil water storage changes across the CONUS at 12.5 km resolution by a Bayesian integration of GRACE data into W3RA. Sci. Total Environ. 758, 143579.
Minallah, S., Ivanov, V.Y., 2019. Interannual variability and seasonality of precipitation in the Indus River basin. J. Hydrometeorol. 20 (3), 379–395.
Moriasi, D.N., Arnold, J.G., Van Liew, M.W., Bingner, R.L., Harmel, R.D., Veith, T.L., 2007. Model evaluation guidelines for systematic quantification of accuracy in watershed simulations. Trans. ASABE 50 (3), 885–900.
Muzammil, M., Zahid, A., Breuer, L., 2020. Water resources management strategies for irrigated agriculture in the Indus Basin of Pakistan. Water 12 (5), 1429.
Muzammil, M., Zahid, A., Breuer, L., 2021. Economic and environmental impact assessment of sustainable future irrigation practices in the Indus Basin of Pakistan. Sci. Rep. 11 (1), 1–13.
Nakaya, T., 2015. Geographically Weighted Regression (GWR) Software. GWR 4.0. ASU GeoDa Center website.
Neitsch, S.L., Arnold, J.G., Kiniry, J.R., Williams, J.R., 2011. Soil And Water Assessment Tool Theoretical Documentation Version 2009. Texas Water Resources Institute.
Panda, D.K., Wahr, J., 2016. Spatiotemporal evolution of water storage changes in I ndia from the updated GRACE-derived gravity records. Water Resour. Res. 52 (1), 135–149.
PARC, 1982. Consumptive Use of Water for Crops in Pakistan. Final Technical Report, 20–30. Pakistan Agricultural Research Council, Islamabad, Pakistan.
Peña-Arancibia, J.L., Stewart, J.P., Kirby, J.M., 2021. Water balance trends in irrigated canal commands and its implications for sustainable water management in Pakistan: evidence from 1981 to 2012. Agric. Water Manag. 245, 106648.
Prakash, S., Gairola, R.M., Papa, F., Mitra, A.K., 2014. An assessment of terrestrial water storage, rainfall and river discharge over Northern India from satellite data. Curr. Sci. 1582–1586.
Qureshi, A.S., 2020. Groundwater governance in Pakistan: from colossal development to neglected management. Water 12 (11), 3017.
Qureshi, A.S., Perry, C., 2021. Managing water and salt for sustainable agriculture in the Indus Basin of Pakistan. Sustainability 13 (9), 5303.
Rodell, M., Chen, J., Kato, H., Famiglietti, J.S., Nigro, J., Wilson, C.R., 2007. Estimating groundwater storage changes in the Mississippi River basin (USA) using GRACE. Hydrogeol. J. 15 (1), 159–166.
Rodell, M., Velicogna, I., Famiglietti, J.S., 2009. Satellite-based estimates of groundwater depletion in India. Nature 460 (7258), 999–1002.
Rodell, M., Famiglietti, J.S., Wiese, D.N., Reager, J.T., Beaudoing, H.K., Landerer, F.W., Lo, M.H., 2018. Emerging trends in global freshwater availability. Nature 557 (7707), 651–659.
Roy, S.S., Rahman, A., Ahmed, S., Ahmad, I.A., 2020. Alarming groundwater depletion in the Delhi Metropolitan Region: a long-term assessment. Environ. Monit. Assess. 192 (10), 1–14.
Samie, A., Abbas, A., Azeem, M.M., Hamid, S., Iqbal, M.A., Hasan, S.S., Deng, X., 2020. Examining the impacts of future land use/land cover changes on climate in Punjab province, Pakistan: implications for environmental sustainability and economic growth. Environ. Sci. Pollut. Res. 27 (20), 25415–25433.
Samimi, M., Mirchi, A., Moriasi, D., Ahn, S., Alian, S., Taghvaeian, S., Sheng, Z., 2020. Modeling arid/semi-arid irrigated agricultural watersheds with SWAT: applications, challenges, and solution strategies. J. Hydrol. 590, 125418.
Santhi, C., Arnold, J.G., Williams, J.R., Dugas, W.A., Srinivasan, R., Hauck, L.M., 2001. Validation of the SWAT model on a large river basin with point and nonpoint sources 1. J. Am.Water Resour.Assoc. 37 (5), 1169–1188.
Scanlon, B.R., Faunt, C.C., Longuevergne, L., Reedy, R.C., Alley, W.M., McGuire, V.L., McMahon, P.B., 2012. Groundwater depletion and sustainability of irrigation in the US High Plains and Central Valley. Proc. Natl. Acad. Sci. 109 (24), 9320–9325.
Scott, C.A., Shah, T., 2004. Groundwater overdraft reduction through agricultural energy policy: insights from India and Mexico. Int.J.Water Resour.Dev. 20 (2), 149–164.
Senay, G.B., Budde, M., Verdin, J.P., Melesse, A.M., 2007. A coupled remote sensing and simplified surface energy balance approach to estimate actual evapotranspiration from irrigated fields. Sensors 7 (6), 979–1000.
Seyoum, W.M., Kwon, D., Milewski, A.M., 2019. Downscaling GRACE TWSA data into high-resolution groundwater level anomaly using machine learning-based models in a glacial aquifer system. Remote Sens. 11 (7), 824.
Shu, J., Shamseldin, A.Y., Weller, E., 2021. The impact of atmospheric rivers on rainfall in New Zealand. Sci. Rep. 11 (1), 1–11.
Simons, G.W.H., Bastiaanssen, W.G.M., Cheema, M.J.M., Ahmad, B., Immerzeel, W.W., 2020. A novel method to quantify consumed fractions and non-consumptive use of irrigation water: application to the Indus Basin irrigation system of Pakistan. Agric. Water Manag. 236, 106174.
Śliwińska, J., Wińska, M., Nastula, J., 2021. Validation of GRACE and GRACE-FO mascon data for the study of polar motion excitation. Remote Sens. 13 (6), 1152.
Smolenaars, W.J., Dhaubanjar, S., Jamil, M.K., Lutz, A., Immerzeel, W., Ludwig, F., Biemans, H., 2021. Future upstream water consumption and its impact on downstream availability in the transboundary Indus basin. Hydrol. Earth Syst. Sci. Discuss. 1–27.
Swarzenski, W.V., 1968. Fresh And Saline Ground-water Zones in the Punjab Region, West Pakistan (No. 1608-I). USGPO.
Tan, M.L., Gassman, P.W., Yang, X., Haywood, J., 2020. A review of SWAT applications, performance and future needs for simulation of hydro-climatic extremes. Adv. Water Resour. 143, 103662.
Tang, Y., Hooshyar, M., Zhu, T., Ringler, C., Sun, A.Y., Long, D., Wang, D., 2017. Reconstructing annual groundwater storage changes in a large-scale irrigation region using GRACE data and Budyko model. J. Hydrol. 551, 397–406.
Umar, M., Khan, S.N., Arshad, A., Aslam, R.A., Khan, H.M.S., Rashid, H., Pham, Q.B., Nasir, A., Noor, R., Khedher, K.M., Anh, D.T., 2022. A modified approach to quantify aquifer vulnerability to pollution towards sustainable groundwater management in irrigated Indus Basin. Environ. Sci. Pollut. Res. 1–22.
Vishwakarma, B.D., Zhang, J., Sneeuw, N., 2021. Downscaling GRACE total water storage change using partial least squares regression. Sci.Data 8 (1), 1–13.
Wang, H., Zang, F., Zhao, C., Liu, C., 2022. A GWR downscaling method to reconstruct high-resolution precipitation dataset based on GSMaP-gauge data: a case study in the Qilian Mountains, Northwest China. Sci. Total Environ. 810, 152066.
Wang, S., Liu, H., Yu, Y., Zhao, W., Yang, Q., Liu, J., 2020. Evaluation of groundwater sustainability in the arid Hexi Corridor of Northwestern China, using GRACE, GLDAS and measured groundwater data products. Sci. Total Environ. 705, 135829.
Watkins, M.M., Wiese, D.N., Yuan, D.N., Boening, C., Landerer, F.W., 2015. Improved methods for observing Earth's time variable mass distribution with GRACE using spherical cap mascons. J.Geophys.Res.Solid Earth 120 (4), 2648–2671.
Watto, M.A., Mugera, A.W., 2016. Groundwater depletion in the Indus Plains of Pakistan: imperatives, repercussions and management issues. Int.J.River Basin Manag. 14 (4), 447–458.
Watto, M.A., Mitchell, M., Akhtar, T., 2021. Pakistan's water resources: overview and challenges. Water Resources of Pakistan, pp. 1–12.
Wiese, D.N., Landerer, F.W., Watkins, M.M., 2016. Quantifying and reducing leakage errors in the JPL RL05M GRACE mascon solution. Water Resour. Res. 52 (9), 7490–7502.
Xiang, L., Wang, H., Steffen, H., Wu, P., Jia, L., Jiang, L., Shen, Q., 2016. Groundwater storage changes in the Tibetan Plateau and adjacent areas revealed from GRACE satellite gravity data. Earth Planet. Sci. Lett. 449, 228–239.
Xie, H., Longuevergne, L., Ringler, C., Scanlon, B.R., 2020. Integrating groundwater irrigation into hydrological simulation of India: case of improving model representation of anthropogenic water use impact using GRACE. J.Hydrol.Reg.Stud. 29, 100681.

Yang, P., Xia, J., Zhan, C., Qiao, Y., Wang, Y., 2017. Monitoring the spatio-temporal changes of terrestrial water storage using GRACE data in the Tarim River basin between 2002 and 2015. Sci. Total Environ. 595, 218–228.

Yang, Z., Dai, W., Yu, W., Shi, Q., Santerre, R., 2021. Mixed geographically and temporally weighted regression for spatio-temporal deformation modelling. Surv. Rev. 1–11.

Yin, W., Hu, L., Zhang, M., Wang, J., Han, S.C., 2018. Statistical downscaling of GRACE-derived groundwater storage using ET data in the North China plain. J.Geophys.Res. Atmos. 123 (11), 5973–5987.

Zeng, C., Yang, L., Zhu, A.X., Rossiter, D.G., Liu, J., Liu, J., Qin, C., Wang, D., 2016. Mapping soil organic matter concentration at different scales using a mixed geographically weighted regression method. Geoderma 281, 69–82.

Zhang, H., Loáiciga, H.A., Ha, D., Du, Q., 2020. Spatial and temporal downscaling of TRMM precipitation with novel algorithms. J. Hydrometeorol. 21, 1259–1278.

Zhang, Y., Li, Y., Ji, X., Luo, X., Li, X., 2018b. Fine-resolution precipitation mapping in a mountainous watershed: geostatistical downscaling of TRMM products based on environmental variables. Remote Sens. 10, 119.

Zhu, Y., Liu, S., Yi, Y., Xie, F., Grünwald, R., Miao, W., Wu, K., Qi, M., Gao, Y., Singh, D., 2021. Overview of terrestrial water storage changes over the Indus River Basin based on GRACE/GRACE-FO solutions. Sci. Total Environ. 799, 149366.

Zuberi, F.A., 1997. Integrated Surface And Groundwater Management Programme for Pakistan-groundwater Resources. Interim Report. IWASRI.